Ore Geology Reviews 112 (2019) 103063

Contents lists available at ScienceDirect

Ore Geology Reviews

journal homepage: www.elsevier.com/locate/oregeorev

The Lazurnoe deposit in the Central Sikhote-Alin, Eastern Russia: Combined shoshonite-related porphyry Cu-Au-Mo and reduced intrusion-related Au mineralization in a post-subduction setting

Serguei G. Soloviev[a,*], Sergey G. Kryazhev[b], Olga V. Avilova[b], Anton V. Andreev[b], Mikhail M. Girfanov[b], Ivan A. Starostin[b]

[a] Institute of Geology of Ore Deposits, Petrography, Mineralogy and Geochemistry (IGEM), Russian Academy of Sciences, 35 Staromonetny Per., Moscow 109017, Russia
[b] Central Research Institute of Geological Prospecting for Base and Precious Metals (TsNIGRI), 1-129 Warshawskoe Chaussee, Moscow 117545, Russia

ARTICLE INFO

Keywords:
Copper
Gold
Porphyry
Shoshonite
Transform margin
Sikhote-Alin
Russia

ABSTRACT

The Lazurnoe porphyry Cu-Au-Mo deposit (> 1Mt Cu-eq.) in the Mesozoic Central Sikhote-Alin orogenic belt (Eastern Russia) is located in an Early Cretaceous turbidite basin associated with a crustal-scale strike-slip fault zone, and was formed under the continental transform margin regime after the cessation of active subduction. The deposit is related to a magnetite-series, high-K calc-alkaline to shoshonitic, Early Cretaceous igneous suite that occurred in this tectonic setting, possibly due to asthenospheric mantle upwelling. The fertile magma was sourced from a subduction-modified mantle, under a low degree of partial melting, and was subjected to intense amphibole fractionation during its crystallization, the latter facilitating water and metal saturation. The parental igneous suite at Lazurnoe was coeval to ilmenite-series calc-alkaline igneous suites accompanied by reduced intrusion-related Au(± W) to W-Au deposits as well as to ilmenite-series, high-K calc-alkaline to shoshonitic suites accompanied by Sn-polymetallic mineralization.

The deposit comprises magnetite-rich, quartz-K-feldspar to quartz-K-feldspar-biotite (potassic) alteration assemblages, containing bornite and chalcopyrite, which evolve to quartz-chlorite ± epidote ± amphibole (propylitic) assemblages, containing dominant pyrite with magnetite and chalcopyrite. Molybdenite-chalcopyrite-pyrite paragenesis dominates in quartz-sericite (phyllic) alteration assemblages that overprint and replace potassic and propylitic alteration. Potassic alteration assemblages formed from hot (~530–510 °C), high-salinity (45–48 wt% NaCl and 9–10 wt% $CaCl_2$), sodic-calcic aqueous-chloride fluid. Gradual fluid cooling and dilution (from 29 to 31 wt% NaCl and 18–19 wt% $CaCl_2$ through 24–25 wt% NaCl and 16–17 wt% $CaCl_2$ to 12 ± 0.5 wt % NaCl and 12 ± 0.5 wt% $CaCl_2$) is recorded for propylitic alteration assemblage. Another cycle of fluid exsolution from crystallizing magma can be suggested for phyllic alteration assemblages formed from a cooler (~390–310 °C), high-salinity (30–37 wt% NaCl and 5 ± 0.5 wt% $CaCl_2$) aqueous-chloride fluid. The porphyry-style mineralization was overprinted by the late auriferous quartz-sulfide veins containing arsenopyrite, pyrrhotite and other sulfide minerals, together with native gold (locally > 100 g/t Au) and tellurides. These veins were formed from boiling aqueous-carbonic fluid that was characterized by elevated CO_2 and CH_4 contents, with subsequent separation of high-carbonic and aqueous-chloride phases, and the fluid cooling from ~390 to 250 °C. These veins can be related to another, more reduced, plutonic suite, which crystallized at a greater depth.

1. Introduction

Alkalic magmatic-hydrothermal systems related to high-K calc-alkaline to shoshonitic igneous suites are recognized to be important in producing significant porphyry Cu-Au-Mo and epithermal Au deposits (Mutschler and Mooney, 1993; Richards, 1995; Jensen and Barton, 2000; Sillitoe, 2002; Soloviev, 2014; Muller and Groves, 2019). Many such igneous suites and associated porphyry Cu-Au-Mo deposits occur in subduction-related settings including island arcs and destructive continental margins (Sillitoe, 2002, 2010; Cooke et al., 2005), with their best studied examples located in the Circum-Pacific magmatic arcs (e.g., Muller and Groves, 2019). However, there is growing evidence indicating development of shoshonite-related porphyry Cu-Au-Mo systems in the post-subduction continental late- to post-collisional

* Corresponding author.
E-mail address: serguei07@hotmail.com (S.G. Soloviev).

https://doi.org/10.1016/j.oregeorev.2019.103063
Received 19 March 2019; Received in revised form 29 July 2019; Accepted 5 August 2019
Available online 08 August 2019
0169-1368/

magmatic arcs as well as at continental transform margins and related crustal-scale strike-slip faults (e.g., Hou et al., 2011; Ludington et al., 2012; Yang et al., 2016; Soloviev, 2014; Moritz et al., 2016; Rezeau et al., 2016; Muller and Groves, 2019). Common for these settings was the generation of fertile magma in the course of partial melting of the metasomatized lithosphere due to asthenospheric mantle upwelling after the cessation of active subduction (Richards, 2009, 2011; Goldfarb et al., 2013).

The Lazurnoe deposit in the Central Sikhote-Alin is recognized as a porphyry Cu-Au-Mo system that formed in a continental transform margin setting occurring after the cessation of an active subduction (Khanchuk et al., 2016; Grebennikov et al., 2016). The deposit remains only partially explored, with resources initially reported as 0.5 Mt of contained Cu-eq. for one of its mineralized zones, with average grades of 0.32% Cu, 0.19 g/t Au and 0.01% Mo (Efimov, 2008). After more drilling and trenching, Naidenko (2013) reported ~1 Mt of contained Cu-eq. Later, Popov et al. (2016) quoted an estimate of 2Mt of contained Cu-eq., and the deposit was listed among the high priority Cu-Au-Mo porphyry targets in the Sikhote-Alin orogenic belt (Petrov et al., 2015; Mihalasky et al., 2015; Ivin et al., 2017). Yushmanov (2009) estimated a 110 t Au endowment for auriferous quartz-sulfide veins and 15–20 t Au in gold placers over the Lazurnoe deposit area. The new geologic, petrologic and fluid inclusion data presented in this paper provide a more detailed view of the deposit formation.

2. Regional tectonic and metallogenic setting

The Lazurnoe deposit is located in the southern part of the Mesozoic Sikhote-Alin orogenic system, a belt that extends for over 1500 km along the NW Pacific coast, is ~600 km wide, and comprises a series of terranes accreted to the eastern Asian continental margin during the Paleozoic and Mesozoic (Fig. 1; e.g., Khanchuk et al., 2016; Grebennikov et al., 2016). Consistently, Khanchuk et al. (2016) distinguished several stages of the tectonic evolution from subduction to transform-like translation of the oceanic plate along the continental margin. In particular, the west-dipping subduction in the Triassic-Late Jurassic (180–145 Ma) was accompanied by the development of the Jurassic accretionary prism. During the Hauterivian-Aptian (145–125 Ma), the transform plate margin was established, with a strike-slip displacement of the early Paleozoic continental blocks, initiation of turbidite basins, intense deformation of the Jurassic and Early Cretaceous terranes, subducted slab break-off and the early asthenospheric mantle upwelling through the slab windows followed by the intrusion of granitoids with mixed crustal-mantle geochemical signatures. The Early Cretaceous turbidite complex is distributed along the boundaries of the Jurassic accretionary prisms, and the corresponding turbidite basins are represented by the Zhuravlevka (in the southern part of the system) and Amur (in the northern part) terranes (Fig. 1). Consistently, from west to east, the Jurassic accretionary prism and the Early Cretaceous turbidite basins are distinguished, the latter reflecting the evolution from subduction to transform-like translation of the oceanic plate along the continental margin (Khanchuk et al., 2016).

During the late Aptian-early Albian (125–115 Ma), the development of the turbidite basins continued, combined with a syn-strike-slip compression caused by a collision with an Early Cretaceous island arc amalgamated to the growing orogenic system from the east. These turbidite basins are composed of Lower Cretaceous (Valanginian to Hauterivian-Aptian) flysh-like (up to 11 km thick) sedimentary sequences comprising sandstones, siltstones and argillites, with conglomerate, gravelite and mixtite horizons, with minor volcanic rocks (Fig. 1; e.g., Malinovsky, 2011; Malinovsky and Golozubov, 2012). In the late Albian-early Cenomanian (115–95 Ma), further development of the transform margin included the intrusion of calc-alkaline magnesian (S- and I-type) and alkali-calcic ferroan (A-type) granitoids into syn-faulting compressional and extensional basins, respectively (Grebennikov et al., 2016). Asthenospheric mantle upwelling through a slab window and subcontinental lithosphere delamination represent the two possible mechanisms to explain the widespread melting of crustal rocks and emplacement of the Early to early Late Cretaceous granitoid suites exhibiting mixed crustal-mantle geochemical signatures, together with more distinctly mantle-related high-K calc-alkaline to shoshonitic, monzogabbro-monzodiorite suites accompanied by trachyandesite-trachybasalt volcanic rocks (Kruk et al., 2014; Jahn et al., 2015). Khanchuk et al. (2016) emphasized the role of the Central Sikhote-Alin strike-slip fault that caused decompression of the upper mantle along a narrow deep-penetrating zone.

The Cretaceous metallogeny of the Central Sikhote-Alin was long time believed to be dominated by tin and tungsten deposits, which are related to different plutonic suites (Fig. 1). In particular, reduced W (W-Au-polymetallic) skarn deposits are related to the Early to early Late Cretaceous (110–95 Ma) ilmenite-series to transitional ilmenite- to magnetite-series granitoid suites (e.g., Soloviev et al., 2017a,b; Soloviev and Kryazhev, 2017). These granitoids are characterized by the involvement of both crustal and mantle-related magmatic sources (Kruk et al., 2014; Jahn et al., 2015). They are followed by slightly younger, ilmenite-series, calc-alkaline granodiorite-granite suites accompanied by Sn-W mineralization (e.g., Gonevchuk et al., 2010). A high-K calc-alkaline to shoshonitic, ilmenite-series, Early to early Late Cretaceous (115–95 Ma) plutonic suite is accompanied by tin-polymetallic (Sn-As-Cu-Zn) mineralization (Gonevchuk et al., 2010, 2011). Recently, a potential of the Central Sikhote-Alin for reduced intrusion-related Au mineralization was recognized (e.g., Soloviev and Krivoschekov, 2011; Soloviev et al., 2017a,b; Soloviev and Kryazhev, 2017), and a number of Au deposits of this style were subsequently delineated (e.g., Sakhno et al., 2013; Gvozdev et al., 2016; Ivin et al., 2017). In total, these deposits constitute a W-Sn-Au metallogenic belt, which follows the Central Sikhote-Alin Fault and corresponds to the development of the region under the continental transform margin regime in the Early and Late Cretaceous (Fig. 1).

The Early to early Late Cretaceous (~100 Ma), principally late Albian-early Cenomanian, was manifested by magnetite-series, dioritic to monzonitic and granitoid intrusions and accompanying discrete clusters of porphyry Cu-Au-Mo mineralization that also form a metallogenic belt aligned with the Central Sikhote-Alin Fault. In particular, these intrusions occur at the Lazurnoe porphyry Cu-Au-Mo deposit in the southern part of the orogenic system (e.g., Sakhno et al., 2011), and at the large Malmyzh porphyry Cu-Au deposit in the northern part of the region (Soloviev et al., 2019; Fig. 1). The latter is associated with the 99–96 Ma intrusions (U-Pb method on zircons; Bukhanova, 2018). Coeval (115–95 Ma) but more reduced (ilmenite-series) monzonitic intrusions are

Subduction resumed in the Late Cretaceous to Paleogene (95–65 Ma), with its subsequent cessation and development of slab-windows channeling ascent of asthenospheric magma (Khanchuk et al., 2016). This resulted in the emplacement of younger (~72–62 Ma) high-K calc-alkaline to shoshonitic suites accompanied by Sn-polymetallic deposits, resembling the Bolivian Sn deposits (Gonevchuk et al., 2005, 2010), and medium-K calc-alkaline to high-K calc-alkaline and shoshonitic suites (~65–35 Ma) accompanied by Pb-Zn and borosilicate deposits (e.g., Vasilenko, 2004).

3. District geology and mineralization

The Lazurnoe deposit area covers a separate cluster of porphyry Cu-Au-Mo and veined/stockwork Au (to Au-W) deposits and occurrences found at the extreme southern (south-western) flank of the much larger Kavalerovo mineral district (Fig. 2A). The district is situated in the Zhuravlevka turbidite basin and is dominated by tin mineralization, with a number of large Sn deposits representing their different types (e.g., Gonevchuk et al., 2005, 2010). These Sn deposits are related to a variety of Early to early Late Cretaceous to Late Cretaceous to Paleogene plutonic suites. The oldest, Early to early Late Cretaceous

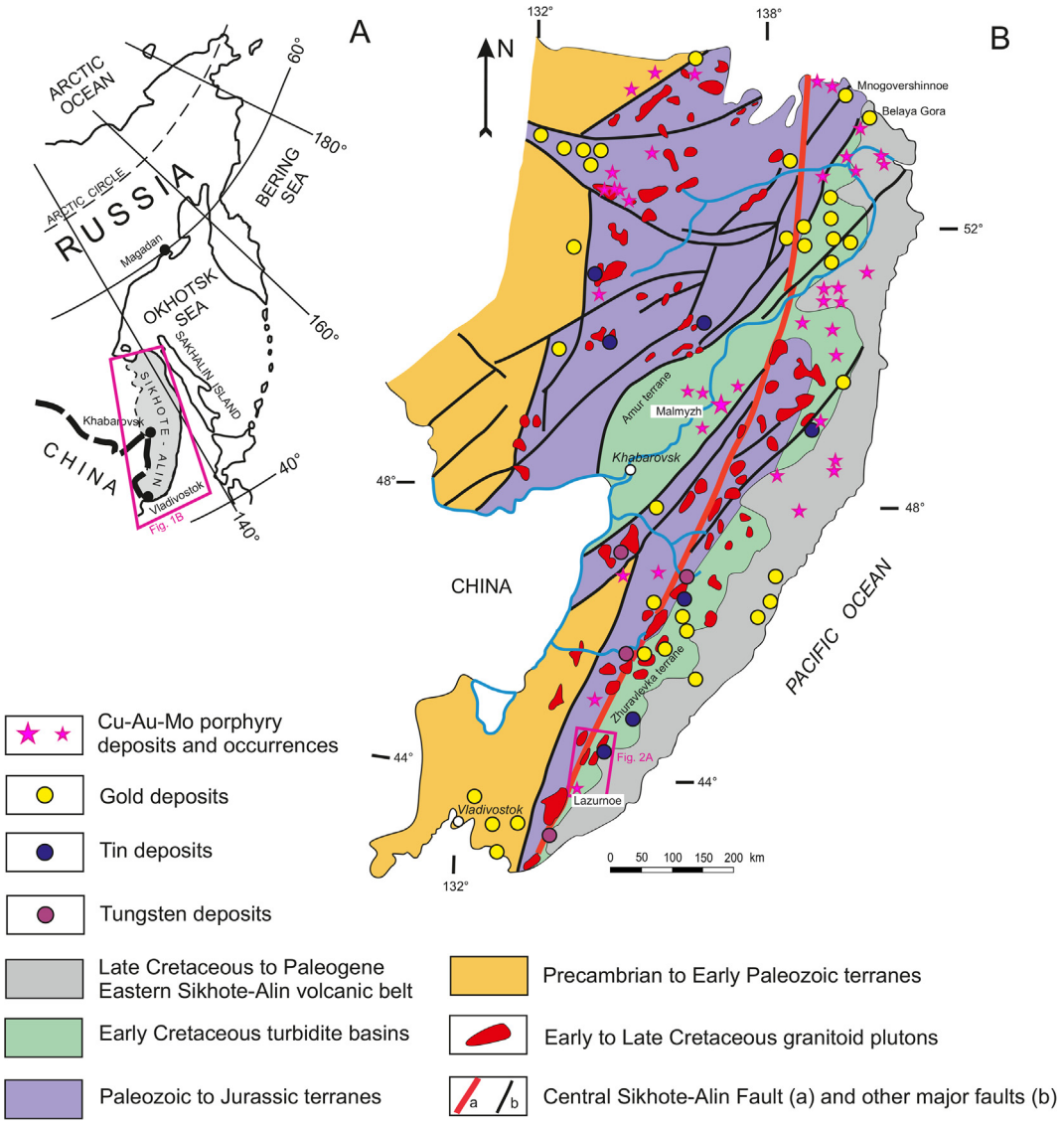

Fig. 1. Position of the Sikhote-Alin orogenic system in the North-West Pacific region (A) and regional tectonic setting of the Lazurnoe and other porphyry Cu-Au-Mo deposits and occurrences, as well as W, Au and Sn deposits, in the Central Sikhote-Alin (B) (geology after Khanchuk et al., 2016; Belyansky et al., 2011).

(120–90 Ma) Berezovsk-Ararat suite is high-K calc-alkaline to shoshonitic, belongs to ilmenite-series, and is accompanied by Sn-polymetallic mineralization (e.g., Arsenievskoe deposit). Coeval picrite-trachybasalt-trachyandesite volcanics are locally present (Kovalenko et al., 1988). The younger Late Cretaceous (100–85 Ma) Uglovsky plutonic suite and Late Cretaceous-Paleocene (85–60 Ma to 70–60 Ma) Shumninsky and other plutonic suites are accompanied by Sn-W and Sn-rare metal (Li, Be, Nb, Ta) mineralization of different types, respectively (Fig. 2A; e.g., Gonevchuk et al., 2005, 2010).

The Lazurnoe deposit area comprises different Cretaceous to Paleogene plutonic and volcanic-plutonic suites (Fig. 2B). These suites include: (1) Early Cretaceous magnetite-series, high-K calc-alkaline to shoshonitic, monzogabbro-monzodiorite-granodiorite suite that should be separated from the nearly coeval but ilmenite-series Berezovsk-Ararat suite, and is below referred to as the Lazurnoe plutonic suite, (2) early Late Cretaceous, transitional magnetite- to ilmenite-series, medium-K calc-alkaline granodiorite-granite suite (Sinancha suite), and (3) Late Cretaceous to Paleogene suite(s) of mafic to intermediate and granitic dikes. In the Lazurnoe plutonic suite, the 110.0 ± 4.0 Ma monzogabbro-monzodiorite of the early intrusive phase was dated by the K-Ar method on amphibole and biotite, whereas the 103.5 ± 1.5 Ma granodiorite of the later intrusive phase was dated by the U-Pb method on zircons (Sakhno et al., 2011). In contrast to the nearly coeval Berezovsk-Ararat igneous suite further north in the Kavalerovo district, the magnetite-series Lazurnoe plutonic suite is accompanied by porphyry Cu-Au-Mo mineralization. Similarly, in contrast to the nearly coeval Uglovsky suite accompanied by Sn mineralization in the rest of the Kavalerovo district, the early Late Cretaceous (95–80 Ma) granodiorite-granite Sinancha suite intrusions in the Lazurnoe deposit area are believe to be accompanied by Au mineralization (Avilova et al., 2016; Gonevchuk et al., 2011).

Gold mineralization in the Lazurnoe deposit area is represented by extended linear quartz-sericite-chlorite-carbonate alteration zones comprising auriferous quartz-sulfide veins. These veins contain native gold associated with pyrite, arsenopyrite, and pyrrhotite, with local chalcopyrite, bismuth minerals, and other sulfides and tellurides. Gold grades vary from fraction of a gram per tonne to > 100 g/t Au (Yushmanov, 2009). These auriferous quartz-sulfide veins may represent one of the most viable sources of large gold placers (Fig. 2B).

4. Deposit geology

The deposit area comprises at least four Cu-Mo-Au mineralized zones associated with separate groups of intrusive stocks likely

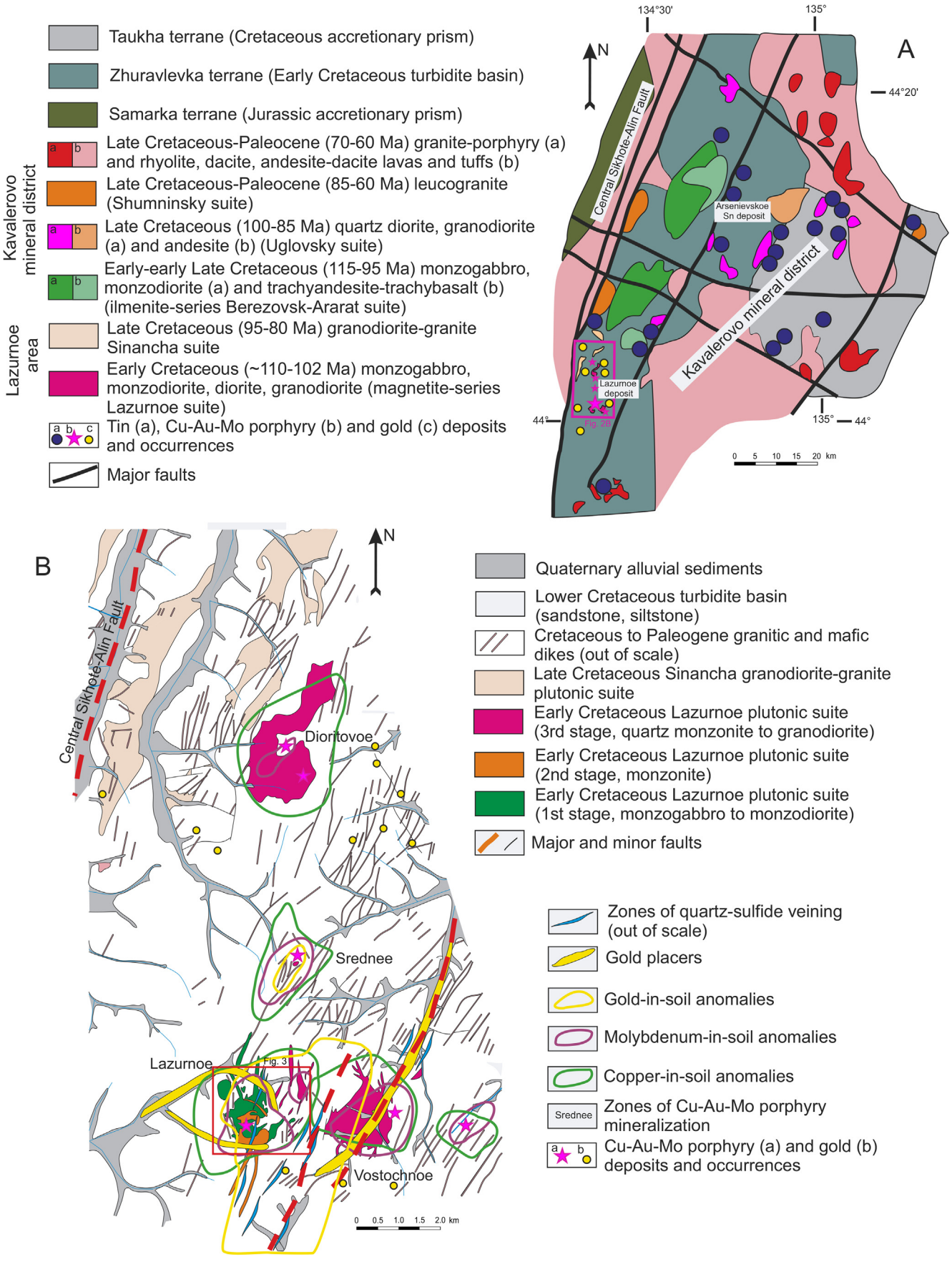

Fig. 2. Geological setting of the Kavalerovo mineralized district comprising the Lazurnoe deposit area (A), and geological map of the Lazurnoe deposit area, showing principal mineralized zones and major intrusions (B) (modified after Avilova et al., 2016; Gonevchuk et al., 2005; Yushmanov, 2001, 2002, 2009).

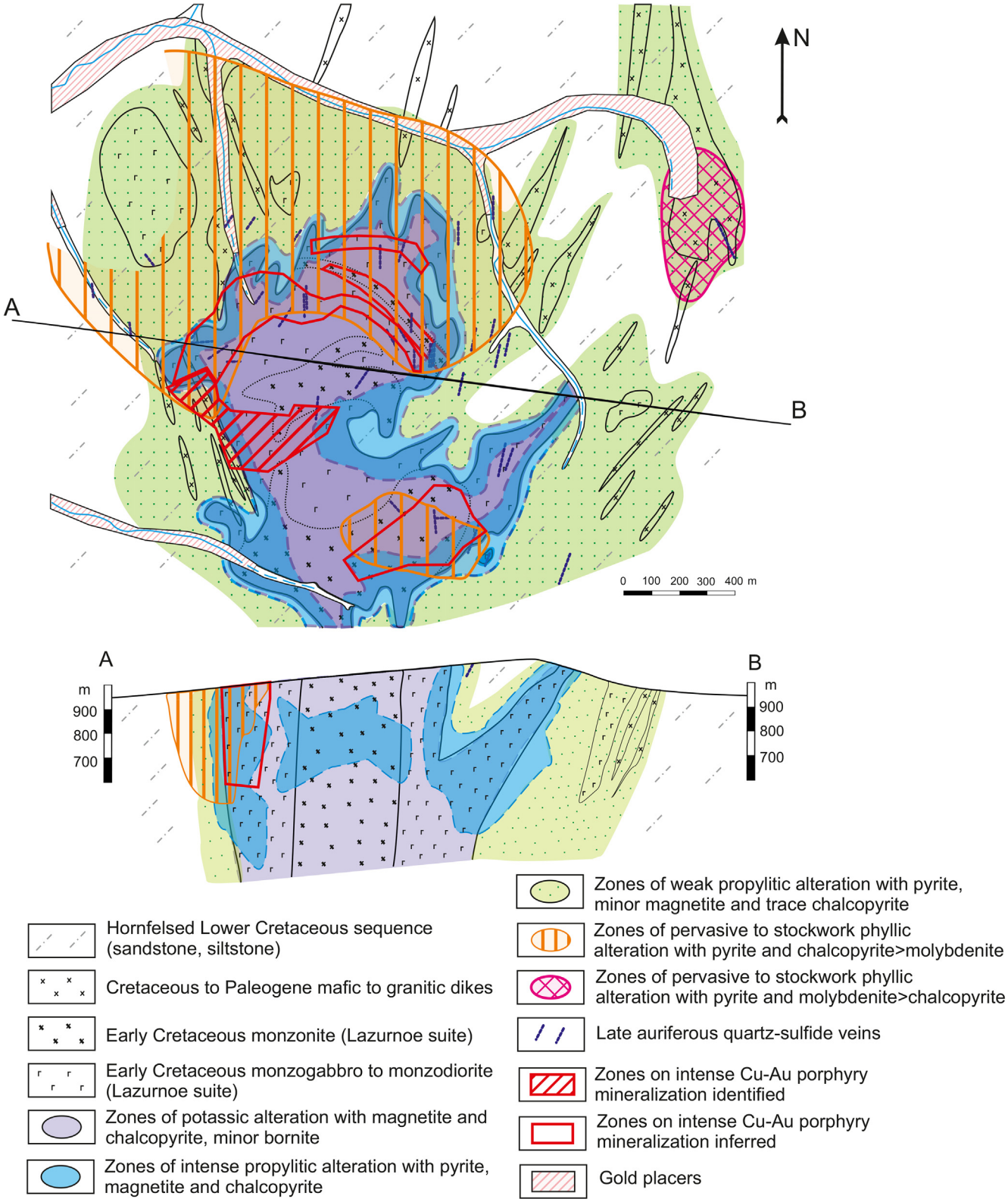

Fig. 3. Geological map and cross-section of the Lazurnoe deposit, with the distribution of hydrothermal alteration assemblages (modified after Avilova et al., 2016; Yushmanov, 2001, 2002, 2009; Efimov, 2008).

representing autonomous magmatic centers ("porphyry centers") (Fig. 2B). Whereas the most explored zone is referred to as the Lazurnoe Zone or the Lazurnoe deposit, the other three zones (i.e., Vostochnoe, Dioritovoe, and Srednee) are underexplored, currently known to contain subeconomic mineralization only, and are considered, by different authors, either as parts ("zones") of the Lazurnoe deposit, or as separate Cu-Mo-Au porphyry-style occurrences within the Lazurnoe deposit area.

The Lazurnoe deposit (or Lazurnoe Zone) covers a nearly isometric pluton (~1.5 km across) composed of several intrusive stocks with

numerous apophyses, and adjacent sedimentary host rocks (Fig. 3). The stocks represent subsequent intrusive (weakly to strongly porphyritic) phases and accompanying dikes; the phases include monzogabbro, monzodiorite and monzonite, with subordinate younger quartz monzonite and granodiorite. A concentric alteration halo overprints the pluton, with the innermost potassic alteration zone containing magnetite and chalcopyrite (and minor bornite), and the outer propylitic alteration zone containing dominant pyrite and chalcopyrite. Large zones of phyllic alteration overprint potassic and propylitic alteration zones in the northern and southern parts of the pluton (Fig. 3). Cu-Au-Mo porphyry mineralization occurs in the endocontact part of the pluton in disconnected zones ~100–300 m wide, in total forming an oval-shaped 1.5 × 1.0 km "ring" zone. It is coincident with the most intense potassic alteration overprinted by propylitic and phyllic alteration. The mineralized zone includes at least two higher-grade intervals bearing chalcopyrite and bornite; they are surrounded by weak pyrite-chalcopyrite mineralization. Mineralization typically contains 0.15–0.30% Cu, with local intervals of 0.4–1% Cu, 0.2–0.3 g/t Au, and 0.0001–0.001% Mo, rarely up to 0.005–0.03% Mo. Yushmanov (2009) reported elevated Pt (0.02–9.34 g/t) and Pd (0.01–2.96 g/t) contents. This mineralization is locally cut by subvertical Au-bearing quartz-sulfide veins, the latter typically being 1–3 m thick and up to 200–300 m long.

The Vostochnoe Zone is associated with a separate pluton, some 1.5 km across, composed mostly of granodiorite-porphyry (Fig. 2B). Phyllic alteration dominates and contains pyrite-molybdenite (with minor chalcopyrite) mineralization, whereas potassic and propylitic alteration is weak. Molybdenum grades range between 0.004 and 0.018%. This mineralization is cut by auriferous quartz-sulfide veins that form 'en echelon' zones, up to several tens of meters across and up to 1.5 km along strike (Yushmanov, 2001). A large gold-scheelite placer is likely related to this late Au mineralization (Fig. 2B).

The Dioritovoe Zone covers another composite pluton comprising monzodiorite to dominant granodiorite (granodiorite-porphyry) stocks (Fig. 2B). These intrusions are overprinted by a zoned hydrothermal alteration halo characterized by a weak chalcopyrite-pyrite-magnetite mineralization in potassic and propylitic alteration zones. The latter contain low grade of 0.02–0.1% Cu, 0.001–0.05 g/t Au, with rare intervals up to 0.1–0.3 g/t Au, and trace Mo (1–2 ppm Mo). More intense mineralization occurs in monzodiorite near the contacts with quartz monzonite and granodiorite. Phyllic alteration forms narrow (from a few centimeters to 2–3 m thick), steeply dipping linear zones overprinting minor parts of potassic and propylitic alteration zones.

The Srednee Zone is characterized by dominant quartz monzonite-, quartz diorite (tonalite)- and granodiorite-porphyry dikes (Fig. 2B) as well as by the presence of abundant breccias with magmatic or hydrothermal cement. Local intervals of potassic alteration, propylitic alteration, and wider intervals of phyllic alteration are present. Cu mineralization (typically 0.1–0.2% Cu) occurs in various hydrothermal assemblages (chalcopyrite-magnetite to pyrite-magnetite-chalcopyrite and dominant pyrite-chalcopyrite paragenesis), and molybdenite is present in propylitic and particularly phyllic alteration assemblages.

5. Analytical methods

The analyses of igneous rocks were performed in the TsNIGRI Labs, Moscow. SiO_2, TiO_2, Al_2O_3, $Fe_2O_{3\ total}$, MnO, MgO, CaO, K_2O, and P_2O_5, were determined by X-ray fluorescence method. FeO was determined by a wet chemical method (volumetric titration). Powdered samples were analyzed by ICP-ES method for trace elements. Analytical errors are 0.5–5% for major elements and 1–10% for trace elements, depending on the concentrations of the respective elements.

Fluid inclusions were studied in samples from the drill core. Twenty six doubly polished sections of 0.3–0.5 mm thick were prepared from 16 individual samples for fluid inclusion petrography and microthermometry. The fluid inclusion study was focused on fluid inclusion assemblages (FIA) of closely associated groups or trails of fluid inclusions with visually similar phase ratios and shapes; this can minimize the effect of homogenization temperature variability of individual inclusions trapped simultaneously, as well as the effect of post-entrapment modifications (Goldstein and Reynolds, 1994). Rare isolated primary fluid inclusions distributed randomly within the core of crystals or forming 3D clusters in different mineral assemblages are most reliable indicators in revealing fluid evolution. Distinguishing of FIA also enables linking groups of fluid inclusions to various mineralizing stages based on their absence in younger mineral assemblages (cf. Masterman et al., 2005). Crosscutting trails of FIA arranged along individual fractures can also reveal the sequence of fluid inclusion entrapment; this includes pseudosecondary trails that are associated with healed microfractures terminated by crystal growth zones (Roedder, 1984).

Microthermometric analyses were made using the UMTK-3 freezing-heating stage designed by VIMS Institute and modified by TsNIGRI Institute, to allow low-temperature experiments. Low-temperature measurements were conducted first; cooling was by liquid N_2 flow. The stage employs a chromel–alumel thermocouple and is capable of attaining temperatures ranging from below −180 to over + 650 °C. The stage was periodically calibrated using the boiling temperature of pure N_2 (−196 °C), triple point for pure CO_2 (−56.6 °C), temperatures of ice melting in standard NaCl solutions (from − 18° to −1 °C), melting temperatures of $AgNO_3$ (210 °C), K_2CrO_7 (398 °C), and NaI (651 °C). Final ice-melting temperatures were accurate to ± 0.2 °C, clathrate melting temperatures to ± 0.5 °C, eutectic temperatures to ± 1.5 °C, and homogenization temperatures to ± 5 °C. Heating rate (at above 30 °C) was 5 °C/min up to a heating limit at 650 °C.

Sulfides for the isotopic study were extracted by a dental drill and/or by the hand picking of chips. Sulfide powders were analyzed by conventional methods using the techniques of Robinson and Kusakabe (1975). Sulfides were decomposed by reaction with CuO at 750 °C, and isotope ratios were measured from SO_2 on a MI-1201 mass spectrometer. Analytical uncertainty of ± 0.2‰ (2 σ) for $\delta^{34}S$ was estimated from internal standards of homogenous pyrite from the Gaiskoe deposit in the Southern Ural ($\delta^{34}S_{VCDT} = +0.7‰$).

6. Igneous rocks of the Early Cretaceous Lazurnoe plutonic suite

The Early Cretaceous Lazurnoe plutonic suite comprises igneous rocks of at least three intrusive stages, with each stage comprising both equigranular and porphyritic rocks representing different intrusive phases based on crosscutting relationships (Table 1). Equigranular rocks are earlier than corresponding porphyry phases and form larger intrusions. In particular, the 1st intrusive stage comprises monzogabbro to monzodiorite; this rock forms a large funnel-like stock in the northern half of the Lazurnoe intrusion (Efimov, 2008; Fig. 3). This melanocratic (dark-grey to dark greenish-grey) medium- to fine-grained rock evolves from dominant equigranular to subordinated weakly porphyritic (with pyroxene phenocrysts) varieties; it contains clinopyroxene dominating over amphibole and biotite (Table 1). The stock is zoned, with its core part composed of monzodiorite (with minor intervals of monzogabbro), and its outer part composed of monzogabbro, with gradual transitions to the monzodiorite in the central part. The equigranular monzogabbro to monzodiorite is accompanied and cut by dikes composed of monzogabbro- to monzodiorite-porphyry, with larger pyroxene, amphibole, biotite and plagioclase phenocrysts, and finer-grained plagioclase-amphibole-biotite groundmass (Fig. 4A; Table 1).

The 2nd intrusive stage comprises equigranular (to weakly-porphyritic) monzonite and monzonite-porphyry (Table 1). Monzonite forms a large stock in the southern half of the Lazurnoe intrusion, which is characterized by numerous elongated apophyses distinctly crosscutting the monzogabbro-monzodiorite of the northern stock (Efimov, 2008; Fig. 3). This melanocratic to mesocratic (dark-grey to dark greenish-grey) medium- to fine-grained rock contains minor

Table 1
Major petrographic features of the Early Cretaceous igneous rocks of the Lazurnoe plutonic suite.

Intrusion stage and phases	Rocks	Petrography
1st stage (phases 1–2 ?)	Monzogabbbro to monzodiorite to monzogabbro- and monzodiorite-porphyry	Medium- to fine-grained melanocratic (dark-grey to dark greenish-grey) rock composed of light-green pyroxene (diopside-augite, enstatite-augite) (20–30 vol%), yellowish-green amphibole (5–15 vol%), biotite (10–15 vol%), plagioclase (labradorite − 35–45 vol% and andesine − 15–20 vol%), and K-feldspar (orthoclase-perthite) (3–7 vol%). Olivine is sporadically present (up to 1–2 vol%). Larger plagioclase grains have distinct zoning from labradorite (in the core) to andesine (rims), and in outer zones contain poikilitic microinclusions of pyroxene, amphibole and biotite. Both equigranular and porphyritic varieties of the rock are present that correspond to different intrusive phases. In turn, pyroxene, amphibole and plagioclase phenocrysts (together up to 40 vol%) are present either together or separately suggesting that there can be different porphyry intrusive phases. Accessory minerals include magnetite (locally up to 3–5 vol%), titanite, apatite and zircon
2nd stage (phases 3–4 ?)	Monzonite to monzonite-porphyry	Medium- to fine-grained melanocratic to mesocratic (dark-grey to dark greenish-grey to pinkish-grey) rock composed of light-green pyroxene (augite) (1–5 vol%), yellowish-green amphibole (15–20 vol%), biotite (10–15 vol%), zoned polysynthetic-twinned plagioclase (andesine-labradorite; 40–60 vol%), and K-feldspar (orthoclase-perthite) (10–25 vol%). Both equigranular and porphyritic varieties of the rock are present that correspond to different intrusive phases. Dominant amphibole and plagioclase phenocrysts are up to 3 mm across form up to 50 vol%, with finer-grained groundmass in porphyry varieties. Accessory minerals include magnetite (locally up to 3–5 vol%), titanite, apatite and zircon
3rd stage (phases 5–6 ?)	Quartz monzonite and quartz diorite (tonalite) to granodiorite to quartz monzonite-porphyry and granodiorite-porphyry	Medium- to fine-grained mesocratic (grey to pinkish-grey) rock composed of yellowish-green amphibole (0–5 vol%), biotite (15–25 vol%), zoned polysynthetic-twinned plagioclase (andesine; 40–50 vol%), and K-feldspar (orthoclase-perthite) (20–25 vol%). Both equigranular and porphyritic varieties of the rock are present that correspond to different intrusive phases. Dominant biotite and plagioclase phenocrysts are up to 3 mm across form typically 25–40 vol%, locally up to 70 vol% in porphyry varieties. Plagioclase phenocrysts are zoned from andesine (with 35–45 mol.% anorthite) in the core to andesine-oligoclase (with 35–25 mol.% anorthite). Both prismatic and rounded to irregularly-shaped (including embayed) quartz phenocrysts are present. Accessory minerals include magnetite, titanite, apatite and zircon

clinopyroxene but dominant amphibole and biotite, together with essential K-feldspar (Fig. 4B and C; Table 1). Amphibole and plagioclase phenocrysts are up to 3 mm across and form up to 50 vol% in monzonite-porphyry.

The 3rd intrusive stage is represented by equigranular quartz monzonite to quartz diorite (tonalite) to granodiorite and accompanying quartz monzonite- to granodiorite-porphyry Fig. 4D and E; Table 1). These rocks form relatively minor dikes that are reported in the southern part of the Lazurnoe intrusion but are present to a greater extent in its northern part and in the Srednee, Vostochnoe and other mineralized zones (Efimov, 2008; Gonevchuk et al., 2009). The medium- to fine-grained stage 3 rocks contain minor amphibole but dominant biotite; phenocrysts in the porphyry varieties are represented mostly by plagioclase and quartz, the latter forming both prismatic and rounded to embayed phenocrysts (Fig. 4F). At the Srednee zone, small but numerous magmatic breccia bodies are present, with a matrix of fine-grained magmatic material (feldspars, biotite, and quartz) resembling quartz diorite or tonalite; these breccias cut across chilled quartz monzonite-porphyry dikes. Gonevchuk et al. (2009) reported small granite-aplite and monzogranite dikes in different magmatic centers.

The whole rock analyses included into the dataset (Table 2) satisfy the criterion on essential immobility of Al and Ti thus supporting the least altered nature of the rocks (Fig. 5A; MacLean and Barrett, 1993). The rocks form a magmatic differentiation trend, ranging from 50 wt% SiO_2 to ~66 wt% SiO_2 (Fig. 5B). More differentiated rocks (including granite-aplite and monzogranite; Gonevchuk et al., 2009) would extend this row toward more siliceous compositions. On the total alkalis vs. SiO_2 diagram (Fig. 5B), the rock plots are arranged along the line dividing the midalkaline and subalkaline fields, as defined by Middlemost (1997). The rocks with lower SiO_2 content (e.g., monzogabbro, monzodiorite, and monzonite) are enriched in K and plot correspondingly in the high-K calc-alkaline to shoshonitic fields (Fig. 5C). In contrast, the rocks with a higher SiO_2 content (quartz monzonite to granodiorite) exhibit a variable K_2O content, and in different magmatic centers are represented either by K_2O-enriched (Lazurnoe and Dioritovoe centers) or K_2O-depleted varieties (Srednee and Vostochnoe centers) (Fig. 5C; Table 2). The Fe_2O_3/FeO ratio is consistently $\gg$0.4, thus indicating oxidized (magnetite series; Ishihara, 1981) intrusions, which correlate with the presence of magnetite as a dominant accessory mineral (Table 1). The rocks are metaluminous and correspond to I-type granites (Fig. 5D; Chappell and White, 1992). On the Rb vs. (Y + Nb) discrimination diagram (Fig. 5E), less fractionated rocks plot as volcanic arc types, whereas more fractionated rocks move toward the syn- and post-collisional granite field (Pearce, 1996), thus displaying the pattern, which reflects a fractionation phenomenon (Pearce et al., 1984). The discrimination diagram of Muller and Groves (2019) designed for high-K igneous rocks (Fig. 5F) indicates the continental subduction-related to post-collisional affinity of the rocks. The Nb/Zr vs. Zr diagram of Thiéblemont and Tegyey (1994) more distinctly indicates a collision-related affinity (Fig. 5G); this, however, should be interpreted toward a post-subduction transform margin development of the region, rather than in favor of actual collisional environment. Elevated Al_2O_3 (> 15 wt%) and high Sr ($\gg$300 ppm) contents, together with low Y contents in the most differentiated rocks, prompted their examination with respect to the adakitic signatures (Fig. 5H and I; Defant and Drummond, 1990; Martin et al., 2005). As a result, the quartz monzonite- and granodiorite-porphyry exhibit some adakitic affinity with respect to the elevated Sr/Y and low Y values (Fig. 5H; cf. Sakhno et al., 2011). On the other hand, the relatively low Yb_N and La_N/Yb_N values are rather inconsistent with an adakitic signature (Fig. 5I). In primitive mantle-normalized trace element spider diagrams (Fig. 5J), the rocks display the lack of Nb anomaly, together with a moderate negative Ta anomaly in the 1st stage rocks, and moderate negative to lacking Ta anomalies in the 2nd and 3rd stage rocks, the latter combined with moderate positive Sr, Zr and Y anomalies. A weak negative Ti anomaly, a strong negative U anomaly, and a strong positive Pb anomaly are also

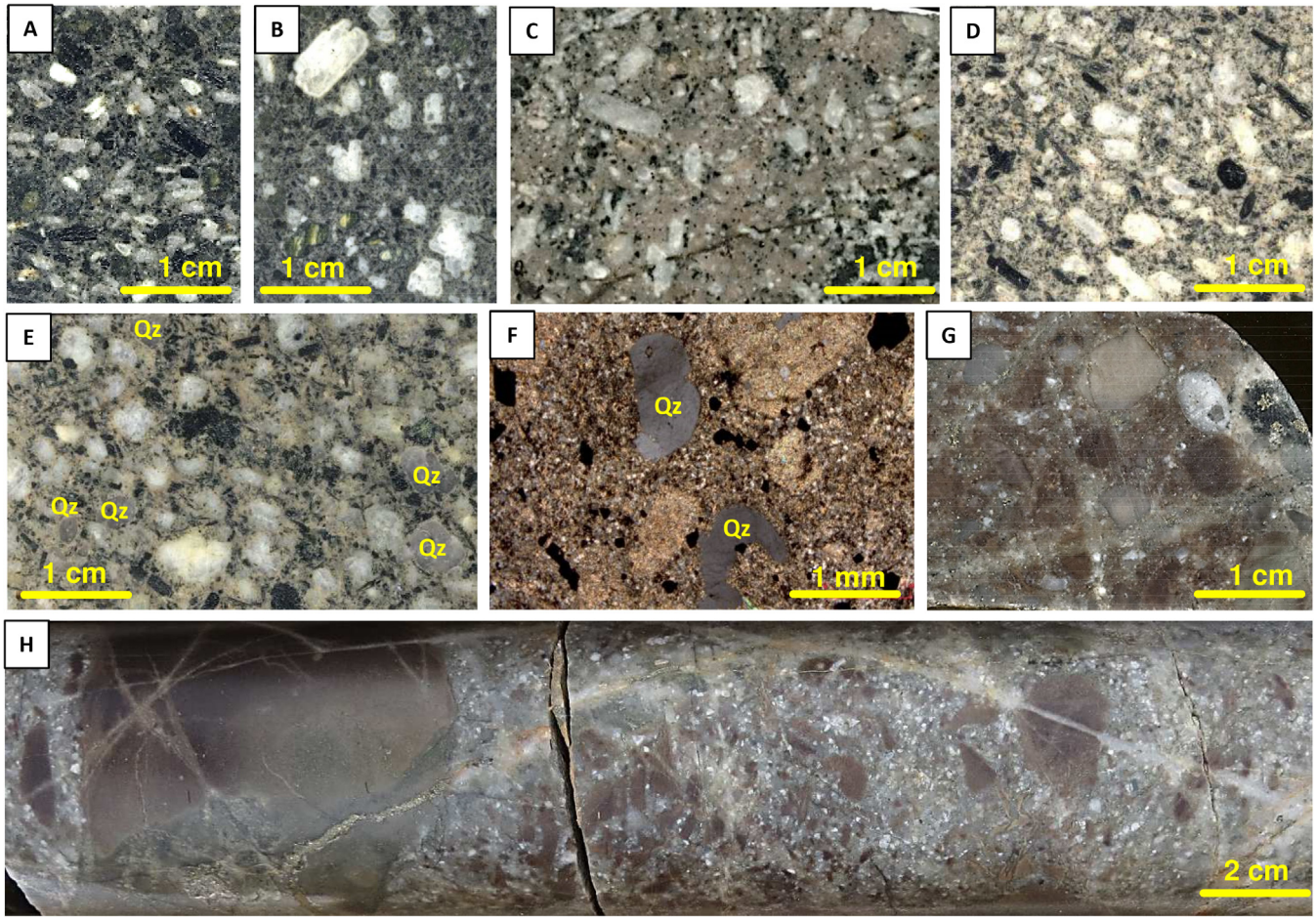

Fig. 4. Photographs showing some typical features of porphyry igneous rocks (porphyry intrusive phases) of the Lazurnoe plutonic suite. A. Monzogabbro-to monzodiorite-porphyry (Lazurnoe Zone; polished slab). B. Monzonite-porphyry (Srednee Zone; polished slab). C. Monzonite-porphyry is overprinted by potassic alteration (pink K-feldspar) (Dioritovoe Zone; polished slab). D. Quartz monzonite-porphyry (Dioritovoe Zone; polished slab). E. Granodiorite-porphyry, with quartz phenocrysts (Srednee Zone; polished slab). F. Granodiorite-porphyry overprinted by phyllic (quartz-sericite-carbonate-pyrite) alteration, with relict embayed quartz phenocrysts (Lazurnoe Zone; thin section, crossed nicols). G-H. Magmatic breccia with quartz monzonite- to granodiorite-porphyry matrix cementing fragments of chert, biotite hornfels, and quartz; both the breccia matrix and fragments are cut by quartz-pyrite veinlets (Srednee Zone; polished slab and drill core). Abbreviations: Qz – quartz. (For interpretation of the references to colour in this figure legend, the reader is referred to the web version of this article.)

recorded. Chondrite-normalized REE diagrams (Fig. 5J) indicate a moderate enrichment in LREE, with a moderately steep overall REE pattern, and no Eu anomalies.

7. Hydrothermal assemblages and mineralization

The hydrothermal mineral paragenesis at Lazurnoe includes potassic, propylitic, and phyllic alteration assemblages constituting a "porphyry cycle" related to the Early Cretaceous magnetite-series, Lazurnoe plutonic suite intrusions, and the late auriferous quartz-sulfide veins with reduced signatures (Fig. 6). Potassic alteration overprints the 1st intrusive stage rocks (monzogabbro to monzodiorite and their porphyry varieties) and is less abundant in the 2nd intrusive stage rocks (monzonite and monzonite-porphyry). Propylitic alteration overprints potassic alteration in the 1st and 2nd intrusive stage rocks, whereas phyllic alteration overprints potassic and propylitic alteration and is most distinctly related to the 3rd intrusive stage rocks (quartz monzonite to granodiorite and their porphyry varieties) and overprints these rocks. The late auriferous quartz-sulfide veins intersect all types of hydrothermal alteration related to the Early Cretaceous intrusions.

7.1. Potassic alteration

This alteration typically occurs in the central (core) parts of the porphyry-related alteration halos, most closely outlines porphyry stocks and overprints both igneous (monzogabbro to monzodiorite, monzonite, and their porphyry varieties) and metasedimentary (siltstone) protolith (Fig. 3). The alteration is represented by wide (up to several hundreds of meters across) zones of pervasive replacement, which incorporate stockworks of variously-oriented veinlets and veins and their coalescing selvages. Zones of pervasive replacement are represented by fine-grained patchy to massive fine-grained quartz-biotite and quartz-K-feldspar-biotite aggregate. In the igneous rocks, phenocrysts of mafic minerals are replaced by fine-grained biotite (with minor magnetite and trace chalcopyrite), whereas plagioclase phenocrysts are progressively replaced by K-feldspar. Dark-green amphibole is locally present as well as calcite and plagioclase (oligoclase) indicating sodic-potassic alteration. In the metasedimentary rocks, the fine-grained quartz-biotite-K-feldspar ± plagioclase alteration is reminiscent of "biotite hornfels".

Zones of pervasive potassic alteration contain numerous quartz-K-feldspar and quartz-biotite veinlets that can be assigned to the A-type (Gustafson and Hunt, 1975). In particular, the earliest are irregularly shaped discontinuous, branching and merging, anastomosing, locally micropegmatitic quartz-K-feldspar veinlets (from fractions of millimeter to several millimeters thick) and veins (1–10 cm thick) (Fig. 7A–D). These veins vary from barren to those containing minor bornite, chalcopyrite and magnetite; magnetite occurs both in their central and outer zones and contains microinclusions of bornite and chalcopyrite

Table 2
Chemical composition of the Early Cretaceous igneous rocks of the Lazurnoe plutonic suite (wt.%, ppm).

Rocks	Monzogabbro to monzodiorite to monzogabbro- and monzodiorite-porphyry				Monzonite to monzonite-porphyry					Quartz monzonite and quartz diorite (tonalite) to granodiorite to quartz monzonite- and granodiorite-porphyry							
Sample numbers	L-010	LK-302–168	LK-304–309	LK-2090	LK-309–146	LK-310–23	LK-312–41	L-018	LK-309–181	LK-311–102	LK-301–53	L-008	LK-2041–1	DK-103–163	DK-58	DR-044	L-020
	1	2	3	4	5	6	7	8	9	10	11	12	13	14	15	16	17
wt percent																	
SiO_2	51.35	52.44	52.08	55.17	59.71	59.84	60.37	60.61	60.98	62.28	62.33	62.54	62.73	63.28	64.30	65.40	66.51
TiO_2	0.72	0.70	0.80	0.66	0.44	0.58	0.44	0.43	0.41	0.41	0.43	0.42	0.38	0.47	0.51	0.49	0.40
Al_2O_3	17.32	17.17	17.05	16.53	15.53	16.09	15.86	16.30	16.44	17.01	15.89	16.56	16.35	15.85	15.90	15.70	15.73
Fe_2O_3	4.71	4.62	4.45	3.83	2.75	2.93	2.58	2.81	3.34	1.91	2.89	2.63	2.80	3.46	2.70	3.38	3.05
FeO	4.48	4.17	4.91	3.77	2.10	2.73	2.29	2.33	1.58	1.55	1.87	1.70	1.66	1.26	1.72	1.41	1.68
MnO	0.21	0.15	0.20	0.16	0.08	0.10	0.07	0.09	0.08	0.08	0.09	0.09	0.07	0.10	0.09	0.06	0.08
MgO	4.82	4.88	4.97	4.33	3.67	3.24	3.35	3.27	2.89	2.08	3.25	2.51	2.81	2.26	2.27	2.10	2.19
CaO	8.67	8.12	8.60	8.12	6.01	4.89	5.97	5.62	5.40	4.95	4.94	3.99	4.16	3.77	4.59	3.70	3.66
Na_2O	2.82	2.96	3.10	3.18	3.82	3.42	3.84	3.85	3.89	4.02	3.90	4.21	4.04	3.85	2.96	2.32	2.94
K_2O	3.12	3.41	2.78	3.14	4.45	4.32	4.36	4.30	4.28	4.33	3.28	4.43	4.56	4.48	4.07	4.10	3.05
P_2O_5	0.45	0.35	0.39	0.35	0.21	0.29	0.23	0.24	0.23	0.23	0.18	0.18	0.16	0.17	0.20	0.20	0.18
LOI	0.64	1.08	0.58	0.41	1.01	1.24	0.87	0.76	0.63	0.97	0.70	0.52	0.40	0.69	0.49	0.84	0.44
Total	99.31	100.05	99.91	99.65	99.78	99.67	100.23	100.61	100.15	99.82	99.75	99.78	100.12	99.64	99.80	99.70	99.91
ppm																	
Ba	461	436	442	483	528	810	555	643	596	685	657	678	708	614	487	512	560
Sr	872	770	786	881	875	832	926	952	905	1070	958	801	923	831	844	813	770
Co	29	25	21	23	16	20	14	13	12	12	17	11	8	12	7.4	9.1	8.6
Ni	24	22	27	31	31	39	29	32	24	22	39	22	24	26	25	20	19
V	245	194	216	213	120	110	114	107	93	89	116	102	114	97	102	89	91
Cr	76	76	55	173	167	94	133	132	125	88	173	143	137	88	72	97	94
Li	7.44	8.12	9.23	9.61	8.38	8.81	7.13	10.1	9.44	9.10	8.54	9.72	8.40	9.54	12.3	10.1	9.67
Rb	73.1	98.0	77.4	92.1	119	79.9	109	110	110	97.0	108	118	115	84.9	101	124	120
Be	1.00	1.09	1.54	1.32	1.50	1.63	1.67	1.10	1.32	2.32	2.34	1.64	1.90	2.34	3.01	2.12	2.31
Zr	98	99	101	98	110	112	146	164	165	172	162	159	141	147	160	165	165
Nb	7	7	8	8	10	10	12	12	13	13	14	13	14	13	14	14	15
Y	22	20	24	22	14	15	16	17	15	15	16	17	18	16	18	21	20
B	3.20	20.1	4.18	3.10	3.93	15.0	5.16	10.4	3.79	7.12	6.85	4.10	3.19	5.56	10.1	22.1	2.34
Sn	< 1.0	< 1.0	1.1	< 1.0	1.2	< 1.0	< 1.0	< 1.0	1.4	2.1	1.0	1.0	< 1.0	< 1.0	2.1	< 1.0	< 1.0
Mo	1.44	1.56	2.23	4.50	6.19	4.99	10.1	1.23	2.23	12.0	1.29	21.0	3.44	1.90	2.12	22.4	2.02
W	< 0.10	< 0.10	0.32	0.37	< 0.10	< 0.10	< 0.10	0.50	0.19	0.11	< 0.10	0.73	0.32	1.01	1.12	0.56	0.60
Cs	2.32	2.12	3.01	2.05	2.35	2.71	2.40	2.18	2.27	1.87	2.02	1.54	1.89	1.23	1.90	1.34	2.59
Hf	2.34	2.60	2.54	2.73	2.50	2.69	3.11	3.14	3.20	3.36	2.15	2.43	2.01	2.88	3.03	3.04	3.11
Ta	0.22	0.21	0.34	0.24	0.22	0.59	0.54	0.69	0.23	0.44	0.49	0.12	0.59	0.25	1.23	0.52	1.31
Ga	12.0	11.3	11.4	12.1	13.3	12.1	11.8	11.2	13.0	11.2	11.0	10.4	11.8	11.9	11.4	10.1	10.8
Ge	1.01	1.45	1.24	1.12	1.20	1.56	1.32	1.39	1.10	1.13	1.34	1.16	1.34	1.29	1.20	1.13	1.19
Th	4.12	4.54	5.02	5.10	4.35	5.82	5.50	7.91	6.10	8.31	7.38	9.10	8.71	9.01	8.98	7.32	8.48
U	1.0	1.1	0.40	0.40	0.50	< 0.1	< 0.1	< 0.1	1.0	0.50	0.60	0.30	0.20	< 0.1	< 0.1	0.30	1.0
Cu	121	409	957	210	2361	490	1662	784	1058	954	274	83	1069	189	410	221	549
Zn	61	63	92	72	37	52	37	37	39	42	43	41	44	41	73	30	82
Pb	18	17	14	19	10	15	17	14	13	25	< 10	12	< 10	20	39	71	15
La	11.9	11.7	12.9	12.7	11.9	12.0	12.3	12.9	13.2	19.2	24.0	12.1	14.1	13.7	13.1	22.1	18.6
Ce	40.1	29.9	53.2	27.2	35.6	38.4	28.2	28.3	28.7	30.1	35.0	26.8	26.5	27.5	25.3	24.8	24.9
Pr	3.88	4.18	4.12	3.81	3.44	3.63	3.42	3.54	2.86	2.81	2.66	2.54	2.74	2.65	2.44	2.32	2.40
Nd	23.3	13.8	22.9	12.4	22.9	22.8	11.9	10.9	10.4	10.0	9.91	10.1	9.53	9.13	8.63	9.10	8.44
Sm	5.10	5.84	4.90	4.74	5.60	4.66	3.40	2.35	2.72	2.52	1.90	2.23	1.98	1.84	1.66	1.70	1.56
Eu	1.18	1.01	0.90	0.88	0.87	0.81	0.82	0.78	0.86	0.74	0.70	0.73	0.66	0.62	0.60	0.71	0.58
Gd	3.44	3.30	2.97	2.80	2.70	2.73	2.63	2.47	2.31	2.54	2.30	1.80	2.10	2.04	2.21	1.99	1.83

(*continued on next page*)

Table 2 (*continued*)

Rocks	Monzogabbro to monzodiorite to monzogabbro- and monzodiorite-porphyry				Monzonite to monzonite-porphyry					Quartz monzonite and quartz diorite (tonalite) to granodiorite to quartz monzonite- and granodiorite-porphyry								
Sample numbers	L-010	LK-302–168	LK-304–309	LK-2090	LK-309–146	LK-310–23	LK-312–41	L-018	LK-309–181	LK-311–102	LK-301–53	L-008	LK-2041–1	DK-103–163	DK-58	DR-044	L-020	
	1	2	3	4	5	6	7	8	9	10	11	12	13	14	15	16	17	
Tb	0.63	0.70	0.66	0.62	0.63	0.51	0.48	0.44	0.50	0.48	0.38	0.43	0.40	0.33	0.32	0.26	0.33	
Dy	2.80	3.10	2.94	2.43	2.29	2.34	2.22	2.19	2.10	1.90	1.92	1.88	1.72	1.83	1.65	1.70	1.61	
Ho	0.53	0.63	0.55	0.51	0.49	0.45	0.40	0.42	0.42	0.49	0.45	0.33	0.35	0.31	0.28	0.30	0.26	
Er	1.38	1.34	1.28	1.44	1.32	1.22	1.10	1.05	1.01	1.12	1.10	1.07	1.07	0.90	0.88	0.73	0.87	
Tm	0.21	0.20	0.20	0.19	0.19	0.18	0.17	0.16	0.15	0.13	0.14	0.14	0.15	0.14	0.13	0.13	0.14	
Yb	1.44	1.32	1.38	1.20	1.21	1.23	1.20	1.19	1.32	1.10	1.55	1.32	1.10	1.13	1.39	1.10	1.07	
Lu	0.10	0.10	0.11	0.12	0.13	0.13	0.14	0.15	0.17	0.17	0.19	0.15	0.16	0.16	0.16	0.17	0.18	

(Fig. 8A). Magnetite is also abundant as background fine dissemination in altered igneous rocks, particularly monzogabbro (up to several percent), where it is associated with fine-grained biotite. Pyrite is locally present in these veins. Copper grades in potassic alteration zones are < 0.3% Cu (mainly 0.1–0.2% Cu); gold grades are typically < 0.1 g/t Au (occasionally 0.1–0.2 g/t Au).

7.2. Propylitic alteration

Two slightly different propylitic alteration zones are distinguished (Fig. 3; cf. Wilson et al., 2003; Corbett, 2017). The “inner” zone is more proximal to the porphyry stocks and overprints outer and upper parts of the potassic alteration zone. Both pervasive replacement and systems of veinlets are developed. Pervasive alteration is expressed in selective replacement of mafic minerals (mainly amphibole and biotite) by chlorite (locally with magnetite and titanite) and feldspars by patchy chlorite-plagioclase-quartz-calcite-magnetite aggregate (Fig. 7F). Quartz veinlets with chlorite (to chlorite-epidote-albite) selvages (Fig. 7G and H) are assigned to propylitic alteration; they intersect quartz-K-feldspar and quartz-biotite veinlets assigned to potassic alteration, thus constraining their relative age. On the other hand, gradual transitions from K-feldspar- and/or biotite-rich (potassic alteration) mineral assemblages to those enriched in chlorite, epidote, and albite have been reported (e.g., Efimov, 2008). Pyrite is much more abundant than that in potassic alteration assemblages, forms fine dissemination both in zones of pervasive replacement and in propylitic veinlets, particularly in close association with chlorite. Chalcopyrite is also associated with propylitic veinlets but is more distinctly related to the pervasive chlorite- and particularly epidote-rich replacement (Fig. 8D). Efimov (2008) reported zones up to 20 m wide comprising chalcopyrite-pyrite mineralization, with the grades varying from 0.3 to 1.5% Cu (averaging 0.5% Cu). Notably these higher-grade intervals occur in local zones of propylitic alteration overprinting potassic alteration (Fig. 3).

The “outer” propylitic alteration zone is more distal and occurs typically > 100 m from the porphyry stock contacts, thus replacing metasedimentary-metavolcanic rocks, and extends locally to > 1 km away from the pluton contacts (Fig. 3). It is generally a pervasive alteration zone, whereas quartz (quartz-chlorite, etc.) veinlets are rare to absent. This alteration is weaker than that in the inner zone and is characterized by relatively more abundant epidote and albite, in expense of chlorite and amphibole that are dominant in the “inner” zone. Also, plagioclase (albite) is locally abundant in the “outer” zone, whereas magnetite is rather rare.

7.3. Phyllic alteration

This alteration appears to be less constrained by a shape of porphyry stocks (or may reflect a shape of hidden parts of the stocks ?) and occurs in various parts of the porphyry-centered alteration systems (Fig. 3). It overprints zones of potassic and propylitic alteration but is also superimposed on previously unaltered metasedimentary rocks. Similar to other alteration types, both pervasive replacement and systems of variously oriented to sheeted veinlets are developed. Pervasive replacement is expressed in the most typical replacement of mafic minerals and feldspars by fine-grained sericite-quartz-carbonate-pyrite aggregate, whereas quartz phenocrysts remain stable (Figs. 4F, 9A). More intense replacement results in the development of sericite-quartz assemblage and finally almost monomineralic quartz including quartz-only veinlets (Fig. 9B–F). Shape of some veinlets is reminiscent of the A- to B-type veins, thus emphasizing the fact that similar vein types can form across different hydrothermal alteration events (Fig. 9F–J; Gregory, 2017; Seedorff et al., 2005). However, K-feldspar and biotite are absent, whereas presence of sericite in selvages and/or occurrence of these veinlets within zones of pervasive, biotite- and K-feldspar-destructive, quartz-sericite replacement distinguishes them from those

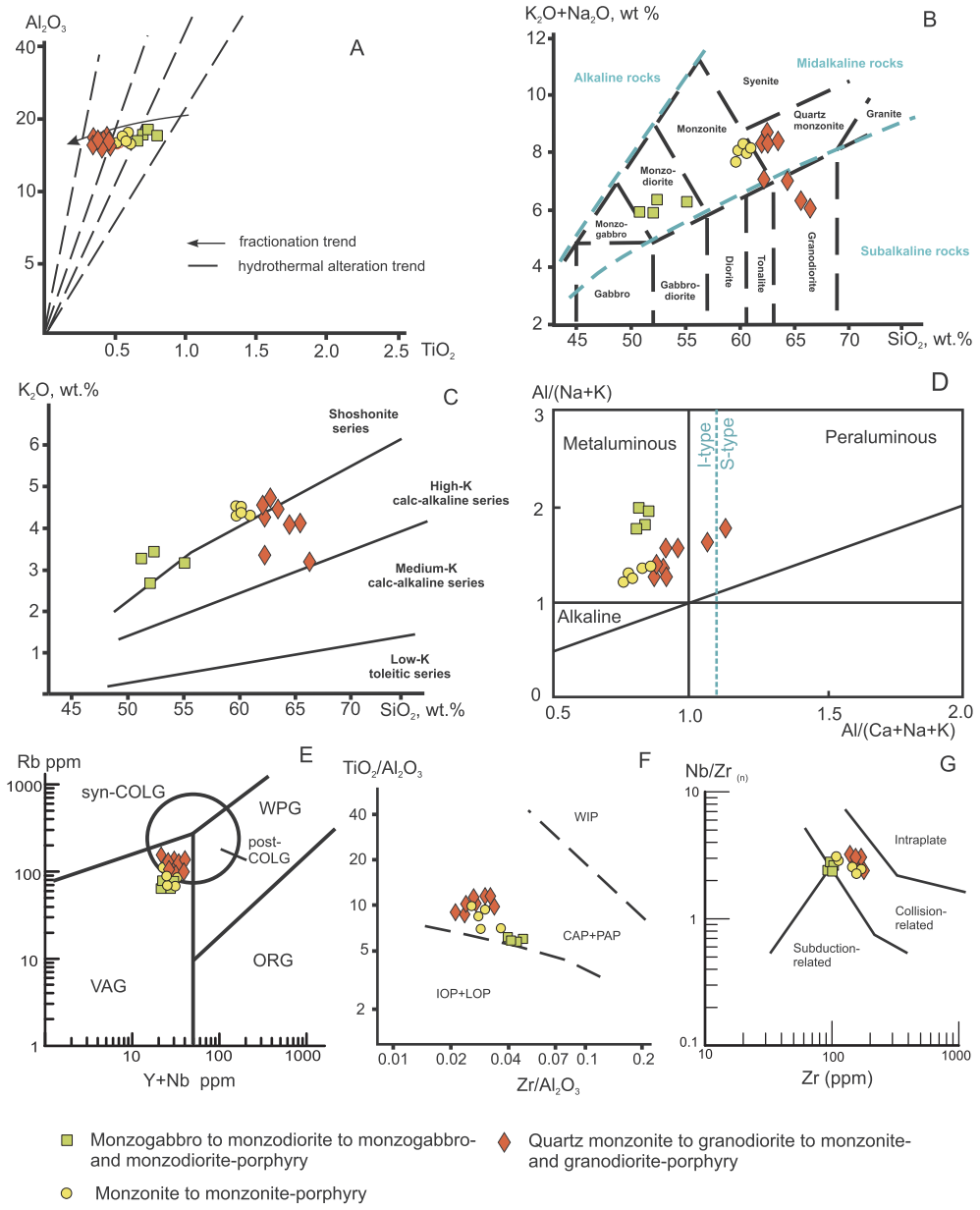

Fig. 5. Plots illustrating the chemistry of igneous rocks of the Lazurnoe plutonic suite. (A) Al_2O_3 vs. TiO_2 diagram showing immobility of Al and Ti in the least altered rock samples (MacLean and Barrett, 1993). (B) SiO_2 vs. (K_2O + Na_2O) diagram for chemical compositions of intrusive rocks (after Le Maitre et al., 1989; Middlemost, 1997). (C) SiO_2 vs. K_2O diagram (after Peccerillo and Taylor, 1976; Le Maitre et al., 1989). (D) Al/(Na + K) vs. Al/(Ca + Na + K) diagram defining the alkaline, metaluminous and peraluminous igneous rocks as well as the I- and S-types of granites (after Maniar and Piccoli, 1989; Chappell and White, 1992). (E) Rb vs. (Y + Nb) diagram showing compositional fields of granitic rocks formed in syncollisional (*syn*-COLG), post-collisional (post-COLG), volcanic arc (VAG), within-plate (WPG), and oceanic ridge (ORG) tectonic environments (after Pearce, 1996). (F) Diagram showing compositional fields of shoshonitic rocks formed in within-plate (WIP), continental arc (CAP) and post-collisional arc (PAP), initial oceanic arc (IAP) and late oceanic arc (LOP) tectonic environments (Muller and Groves, 2019). (G) Nb/Zr vs. Zr diagram showing compositional fields of igneous rocks formed in subduction-related, collision-related and intraplate tectonic environments (Thiéblemont and Tegyey, 1994). (H-I) Sr/Y vs. Y and La_N/Yb_N vs. Yb_N diagrams showing compositional fields of adakite and normal calc-alkaline arc rocks (after Defant and Drummond, 1990; Martin et al., 2005; data normalized by REE contents in Cl carbonaceous chondrite after McDonough and Sun, 1995). (J) Primitive mantle-normalized extended trace element spider diagrams (normalization with respect to Sun and McDonough, 1989) and rare earth element chondrite-normalized diagrams (normalization with respect to McDonough and Sun, 1995). The individual rock compositions are from Table 2.

assigned to potassic alteration. Minor chlorite is present mostly in association with carbonates (and locally albite) in zones of pervasive replacement or in the outermost selvages of the veinlets. Carbonates include both calcite and Fe-Mg carbonates (siderite, ankerite, dolomite); trace tourmaline is locally present.

Hydrothermal breccia observed at the Srednee Zone is cemented fine-grained and cryptocrystalline hydrothermal quartz-albite-sericite-pyrite matrix resembling phyllic alteration assemblage (Fig. 9D), whereas magmatic breccia with quartz monzonite- to granodiorite-porphyry matrix is cut by quartz-sericite-pyrite veinlets (Fig. 9E). The breccias comprise angular to rounded fragments of sedimentary host rocks (siltstone, sandstone, argillite, quartzite, chert, mafic volcanic rocks) and fragments of minerals (quartz, feldspars) that vary in size from a fraction of a centimeter to several centimeters across. Some fragments were subjected to hornfelsing and/or potassic alteration (with dominant biotite) prior to brecciation. Fragments of propylitic-altered rocks (with chlorite-magnetite-pyrite aggregate) are also present.

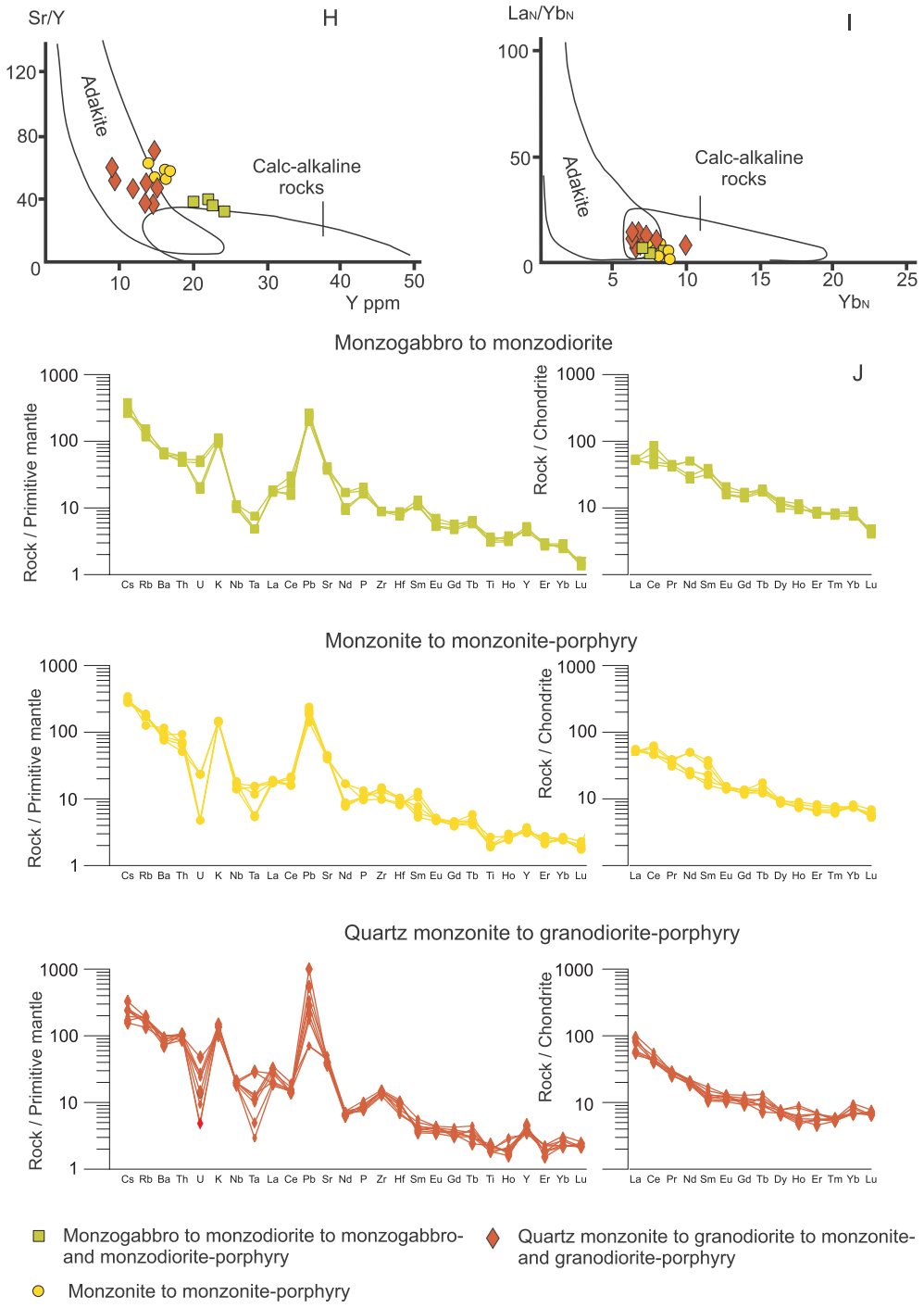

Fig. 5. (*continued*)

Pyrite is the most abundant sulfide mineral in phyllic alteration assemblages and, together with chalcopyrite and/or molybdenite, forms fine dissemination of mostly cubic crystals in the pervasively altered igneous rocks and in thin (typically < 5 mm) veinlets. Chalcopyrite and molybdenite are irregularly distributed forming both fine dissemination in zones of pervasive replacement as well as larger (1–3 cm across) aggregates in quartz-sericite veinlets. Quartz-molybdenite veinlets typically assigned to the type-B (Gustafson and Hunt, 1975) appear to be younger than quartz-pyrite and quartz-pyrite-molybdenite veinlets that correspond to the A-type or transitional AB-type (Fig. 9G–I). Consistently, phyllic alteration overprint of potassic and propylitic alteration zones can result in either Cu grade increase or dilution. More typically, phyllic alteration overprint contributes to Mo (up to 0.5%) and/or Au (typically fractions of gram per tonne) grade increase.

7.4. Late auriferous quartz-sulfide (quartz-carbonate-sericite-sulfide) veins

The late quartz-sulfide veins cut across igneous and sedimentary rocks and follow transverse steeply dipping linear fracturing zones (Fig. 2). At least 30 large quartz-sulfide veins up to 2 m thick have been encountered in the Lazurnoe Zone (Yushmanov, 2002, 2009; Avilova et al., 2016), although the largest veins appear to be situated outside of porphyry-style alteration and mineralization zones. Their central parts are composed of monomineralic quartz (1–2 cm to 1 m thick) or quartz-carbonate aggregate (Fig. 9K–L) that is surrounded by sericite-albite-

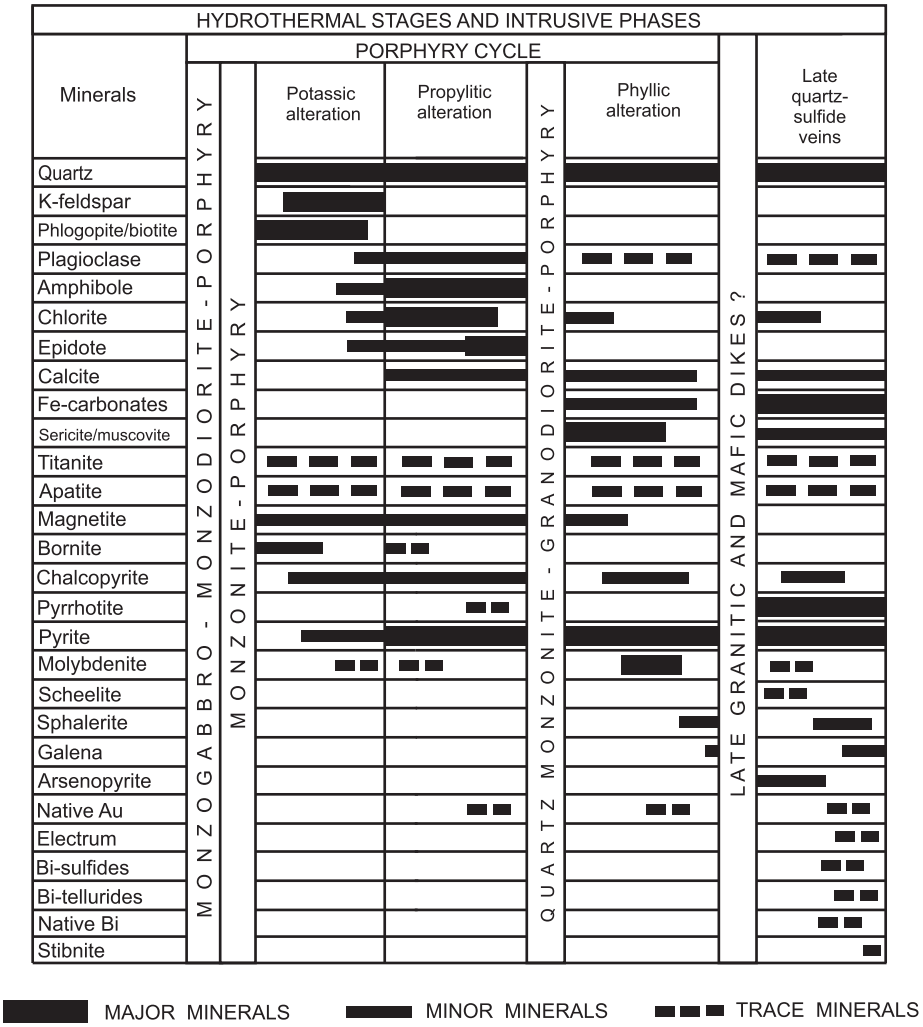

Fig. 6. Sequence of hydrothermal alteration assemblages and intrusive phases at the Lazurnoe deposit.

carbonate selvages (with minor chlorite, trace tourmaline and fluorite). Quartz-carbonate aggregate locally cements zones of multiple tectonic breccia. Sulfide minerals, besides pyrite and minor chalcopyrite, include locally abundant arsenopyrite, sphalerite and galena, and trace stibnite. Scheelite is locally present. Various sulfosalts, Bi minerals, electrum (Fig. 8F) and often coarse native Au (fineness 700–900‰; Yushmanov, 2009) occur, in total contributing to locally high Au (up to 100–300 g/t Au) and Ag (up to several hundreds g/t Ag) grades. Yushmanov (2009) reported quartz-sulfide veins extending for 1.5 km along strike and being up to 0.9 m thick in their central parts that contain 8.7–58.0 g/t Au. Central parts of the veins are surrounded by a stockwork halo (of thin branching, locally sheeted veinlets paralleling the central vein) containing up to 2.8 g/t Au over 11.8 m (Yushmanov, 2009). In total, these veins overprinting zones of the porphyry-related alteration and mineralization can provide significant enrichment in Au and Ag.

8. Fluid inclusion analysis

Fluid inclusions in minerals from the Lazurnoe deposit were initially studied by Gonevchuk et al. (2009), who identified main types of fluid inclusions and defined their P-T-X characteristics. We focused on fluid inclusion assemblages assigned to different hydrothermal alteration assemblages (Table 3).

8.1. Fluid inclusions in quartz from quartz-K-feldspar ± biotite veinlets (potassic alteration)

Primary and pseudosecondary multisolid type 1 fluid inclusions are present as isolated individuals and in short trails (Fig. 10A–D). These inclusions contain 15–20 vol% gas bubble and several solid phases in total occupying up to 75 vol%. The solids include halite and 2–3 anisotropic and highly to weakly birefringent solid phases (including a colorless prismatic crystal with negative extinction, possibly apatite), and a small opaque solid phase. On freezing/warming, type 1 inclusions show eutectic melting temperatures of −65 °C, which would be indicative of dominant LiCl (Borisenko, 1977; Crawford, 1981), but, under absence of any lithium mineralization, is rather explained by a metastable state of the $CaCl_2$-NaCl-H_2O system at low temperatures (Davis et al., 1990; Samson and Walker, 2000). Final ice melting temperatures vary from –33 to −30 °C. Thus, it can be suggested that type 1 inclusions contain $CaCl_2$ and NaCl. On heating, type 1 inclusions exhibit disappearance of the gas bubble at 350–380 °C and dissolution of halite at 430–455 °C (Table 3). The latter, in the NaCl-$CaCl_2$-H_2O system, yields concentrations of 45–48 wt% NaCl and 9–10 wt% $CaCl_2$ (Vanko et al., 1988; Oakes et al., 1990; Fig. 11A). Upon further heating, type 1 inclusions decrepitated at 530–560 °C. Other solid phases in type 1 fluid inclusions remain undissolved over the entire range of heating.

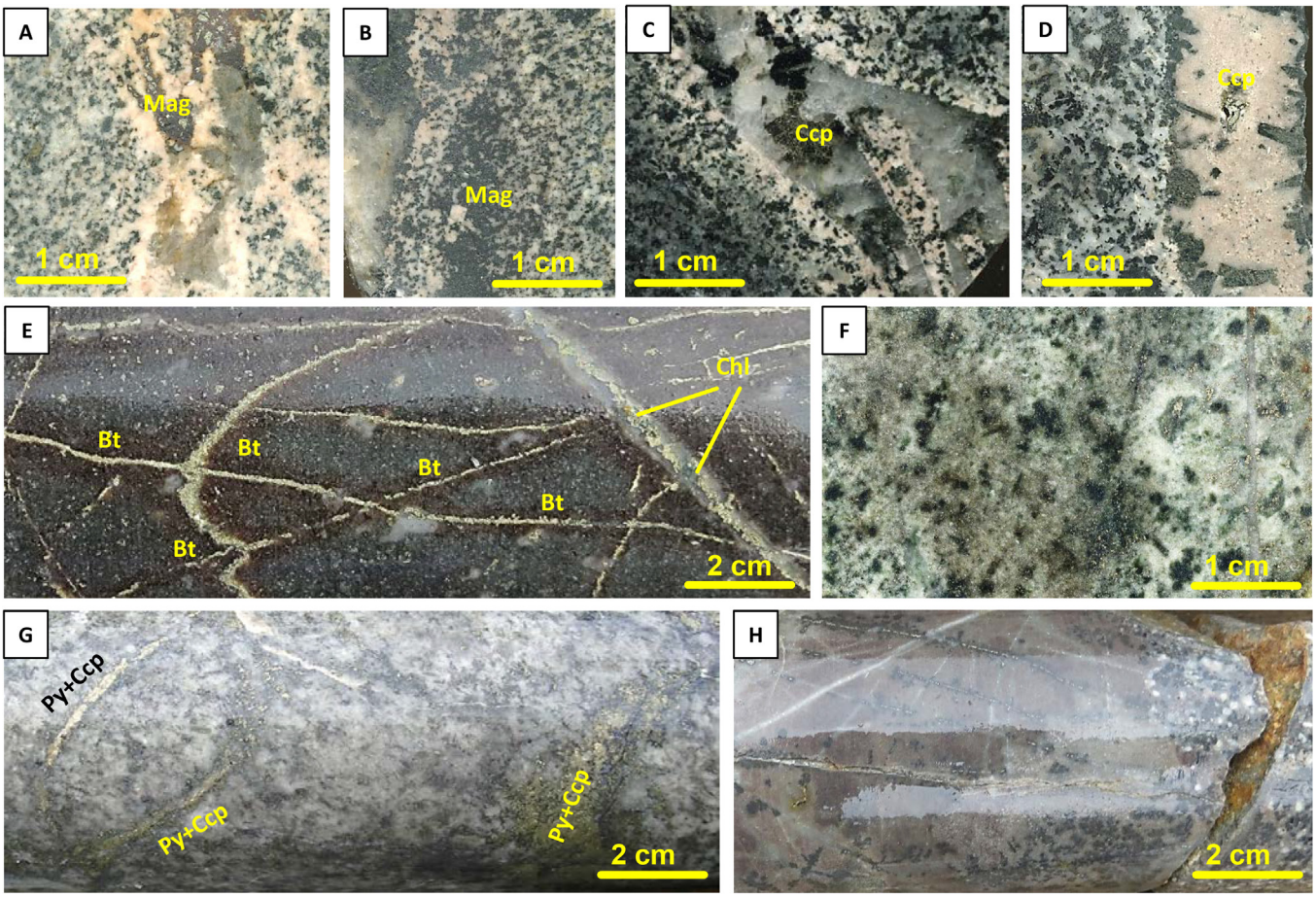

Fig. 7. Photographs showing some typical features of potassic and propylitic alteration assemblages in the Lazurnoe deposit area. A. Quartz-K-feldspar veinlets contain magnetite-chalcopyrite aggregate (Lazurnoe Zone; polished slab). B. Quartz-K-feldspar veinlet in monzodiorite is accompanied by fine-grained magnetite dissemination (Lazurnoe Zone; polished slab). C. Pegmatite-like coarse-grained quartz-biotite veinlets with diffuse K-feldspar selvages in monzodiorite (Dioritovoe Zone; polished slab). D. K-feldspar-biotite (partially replaced by amphibole) veinlet in monzodiorite; chalcopyrite is present in the axial part of the veinlet (Dioritovoe Zone; polished slab). E. Quartz-chalcopyrite-pyrite veinlets with biotite selvages cut monzogabbro-porphyry and are cut by quartz-chlorite-chalcopyrite-pyrite veinlets (Lazurnoe Zone; drill core). F. Pervasive propylitic alteration with patchy chlorite and fine-disseminated magnetite in monzonite-porphyry (Lazurnoe Zone; polished slab). G. Quartz-chlorite-pyrite-chalcopyrite veinlets in propylitic-altered monzonite (Lazurnoe Zone; drill core). H. Zone of potassic (quartz-biotite) alteration cut by quartz-chlorite veinlets and replaced by patchy chlorite aggregates is cut by quartz monzonite-porphyry (Lazurnoe Zone; drill core). Abbreviations: Ccp – chalcopyrite, Mag – magnetite, Bt – biotite, Chl – chlorite.

8.2. Fluid inclusions in quartz from quartz-chlorite ± epidote ± amphibole veinlets (propylitic alteration)

Primary and pseudosecondary multisolid type 2 fluid inclusions are present as isolated individuals and in small isolated clusters (Fig. 10E-H). They are characterized by similar temperatures of the gas bubble homogenization (280–310 °C) but by different salinities. In particular, subtype 2–1 and 2–2 fluid inclusions contain a small (10–15 vol%) gas bubble and several solid phases in total occupying 15–40 vol%; the solids include halite and 1–2 anisotropic and highly to weakly birefringent solid phases, and a small opaque solid phase. On freezing/warming, both subtype 2–1 and 2–2 inclusions show eutectic melting temperatures of −65 °C, which would be indicative of dominant LiCl (Borisenko, 1977; Crawford, 1981). Similar to type 1 inclusions in quartz from potassic alteration assemblage, under any lithium mineralization lacking, this eutectic temperature is rather explained by a metastable state of the $CaCl_2$-NaCl-H_2O system under low temperatures (Davis et al., 1990; Samson and Walker, 2000). The difference of subtype 2–1 and 2–2 fluid inclusions is in their contrasting final ice melting temperatures that is −50 to −48 °C in subtype 2–1 fluid inclusions and −35 to –33 °C in type 2–2 fluid inclusions (Table 3). On heating, both subtype 2–1 and 2–2 inclusions exhibit disappearance of the gas bubble at 280–310 °C, whereas dissolution of halite occurs at 325–335 °C in subtype 2–1 inclusions, and at 250–260 °C in subtype 2–1 inclusions. This, in the NaCl-$CaCl_2$-H_2O system, yields concentrations of 29–31 wt % NaCl and 18–19 wt% $CaCl_2$ for subtype 2–1 inclusions, and 24–25 wt % NaCl and 16–17 wt% $CaCl_2$ for subtype 2–2 inclusions (Vanko et al., 1988; Oakes et al., 1990; Fig. 11A).

Subtype 2–3 fluid inclusions contain a larger (20–25 vol%) gas bubble and occasionally a small opaque solid phase (Fig. 10H). On freezing/warming, subtype 2–3 inclusions show eutectic melting temperatures of −60 °C and final ice melting temperatures of –23 to –22 °C (Table 3). On heating, subtype 2–3 inclusions exhibit disappearance of the gas bubble at 280–310 °C. Considering the NaCl-$CaCl_2$-H_2O system, concentrations of 12 ± 0.5 wt% NaCl and 12 ± 0.5 wt% $CaCl_2$ can be estimated for subtype 2–3 inclusions (Vanko et al., 1988; Oakes et al., 1990; Fig. 11A). In total, a long evolutional trend toward lower NaCl and $CaCl_2$ concentrations can be suggested for subtype 2–1, 2–2 and 2–3 inclusions (Fig. 11A). Other solid phases in type 2 fluid inclusions remain undissolved to 480 °C, when the inclusions decrepitated.

8.3. Fluid inclusions in quartz from quartz-sericite-sulfide veinlets (phyllic alteration)

Primary and pseudosecondary type 3 fluid inclusions contain a small (10–15 vol%) gas bubble and a halite crystal; one or two

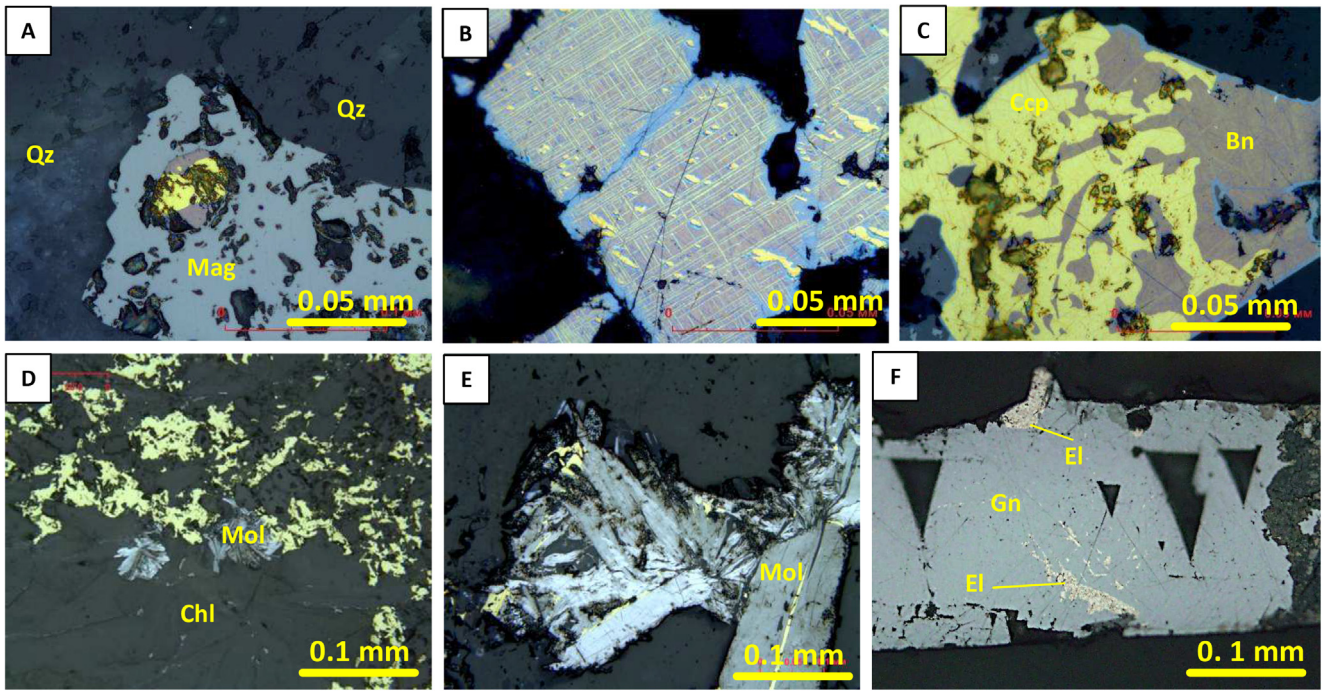

Fig. 8. Photomicrographs of polished sections showing relationships of minerals in the Lazurnoe deposit area. A-F. Potassic alteration: A. Magnetite contains inclusions of bornite and chalcopyrite (Dioritovoe Zone). B. Bornite-chalcopyrite solid solution breakdown (Lazurnoe Zone). C. Chalcopyrite-bornite intergrowths (solid solution breakdown) (Lazurnoe Zone). D. Propylitic alteration: G. Fine-disseminated chalcopyrite and molybdenite in chlorite aggregate (Lazurnoe Zone). E. Phyllic alteration. Coarse molybdenite (with minor chalcopyrite) in a quartz veinlet (Lazurnoe Zone). F. Electrum in galena from late quartz-sulfide vein (Lazurnoe Zone). Abbreviations: Mag – magnetite, Bn – bornite, Ccp – chalcopyrite, Mol – molybdenite, Gn – galena, El – electrum, Qz – quartz, Chl – chlorite.

anisotropic phase(s), and small magnetic (magnetite ?) to non-magnetic opaque phases are observed occasionally, possibly in the inclusions subjected to the post-entrapment modifications (Fig. 10I-K). On freezing/warming, type 3 inclusions exhibit eutectic melting temperatures at −55 °C (indicating the presence of $CaCl_2$ and NaCl; Crawford, 1981); final ice melting temperatures are –23 to –22 °C. On heating, the gas bubble disappears at 150–230 °C, and halite dissolves at 230–310 °C (Table 3). The latter, in the NaCl-$CaCl_2$-H_2O system, yields concentrations of 30–37 wt% NaCl and 5 ± 0.5 wt% $CaCl_2$ (Vanko et al., 1988; Oakes et al., 1990; Fig. 11A). Other solid phases occasionally observed in type 3 fluid inclusions remain undissolved to 350–400 °C, when the inclusions decrepitated.

8.4. Fluid inclusions in quartz from the late auriferous quartz-sulfide veins

A different FIA was identified in quartz from the late quartz-sulfide veins (Table 3). It is represented by aqueous-carbonic type 4 inclusions comprising coexisting fluid inclusions of two subtypes, namely, by gaseous (90–95 vol% gas) subtype 4A and liquid-gaseous (50–40 vol% gas) subtype 4B inclusions (Fig. 10M and N; Table 3). These fluid inclusions most typically form variously sized isolated clusters. On warming after freezing, subtype 4A inclusions exhibit presence of a carbonic phase that melts at −59.5–−58.5 °C and homogenizes into gas at +17 to +19 °C (Table 3). This corresponds to a CH_4 mole fraction of 0.15 (CO_2:CH_4 = 85:15; Thiery et al., 1994). Subtype 4A inclusions show clathrate melting at +7.5 to +8.5 °C that, in the NaCl-CO_2-H_2O system, indicates a salinity of 3–5 wt% NaCl-eq. (Darling, 1991). Subtype 4B inclusions, on freezing/warming, exhibit eutectic melting temperatures at around −29 to −25 °C (indicating $MgCl_2$-NaCl-KCl to $MgCl_2$-NaCl mixture; Crawford, 1981). Final ice melting in subtype 4B inclusions occurs at −6.5 to −4.5 °C, whereas clathrate melts at + 4.5 to 5.5 °C. In the NaCl-H_2O and NaCl-CO_2-H_2O systems, it corresponds to a salinity of 7.2 to 9.9 wt% NaCl-eq. (Bodnar and Vityk, 1994; Darling, 1991). On heating, subtype 4A inclusions homogenize to gas at 350–390 °C, whereas subtype 4B inclusions homogenize to liquid at 340–380 °C (Table 3).

Primary and pseudosecondary aqueous liquid-gaseous type 5 fluid inclusions are typically isolated, or form short trails (Fig. 10O). These inclusions contain a small (20–25 vol%) gas bubble and, on freezing/warming, exhibit eutectic melting temperatures at −27.5 to −26.5 °C (indicating a $MgCl_2$-NaCl-KCl to $MgCl_2$-NaCl mixture; Crawford, 1981); final ice melting temperatures are −7.3 to −3.5 °C. On heating, type 5 inclusions homogenize to liquid at 250–295 °C (Table 3). Salinity estimates for the NaCl-H_2O system, based on the ice melting temperatures, indicate a salinity of 5.7–10.9 wt% NaCl-eq. (Bodnar and Vityk, 1994; Table 3).

8.5. Pressure estimate

Minimum pressure can be estimated using homogenization temperatures of multisolid type 1, 2 and 3 fluid inclusions that reached final homogenization by halite dissolution. Using the isochores for a 30–50 wt% NaCl solution (Atkinson, 2002; Becker et al., 2008), these estimates yield minimum pressures of 850 ± 50 bars for type 1 inclusions, 400 bars for type 2 inclusions, and 850 ± 50 bars for type 3 inclusions (Fig. 11B–D; Table 3). The pressures of 850 ± 50 bars correspond to depths of about 3.5 km (cf. Fournier, 1999) assuming lithostatic conditions. The pressure of 400 bars estimated for type 2 inclusions corresponds to their measured homogenization temperature (325–335 °C), whereas, for the entrapment temperature of 360–380 °C, the pressure would be at around 850 ± 50 bars, which is similar to the pressures estimated for the other porphyry hydrothermal stages (Fig. 11C).

The presence of coexisting gaseous type 4A and aqueous-gaseous type 4B inclusions in the same clusters and trails supports their contemporaneous entrapment in the two-phase immiscibility field. If so, the trapping pressures for these fluid inclusions can be established using the respective trapping temperatures for the high-density fluid

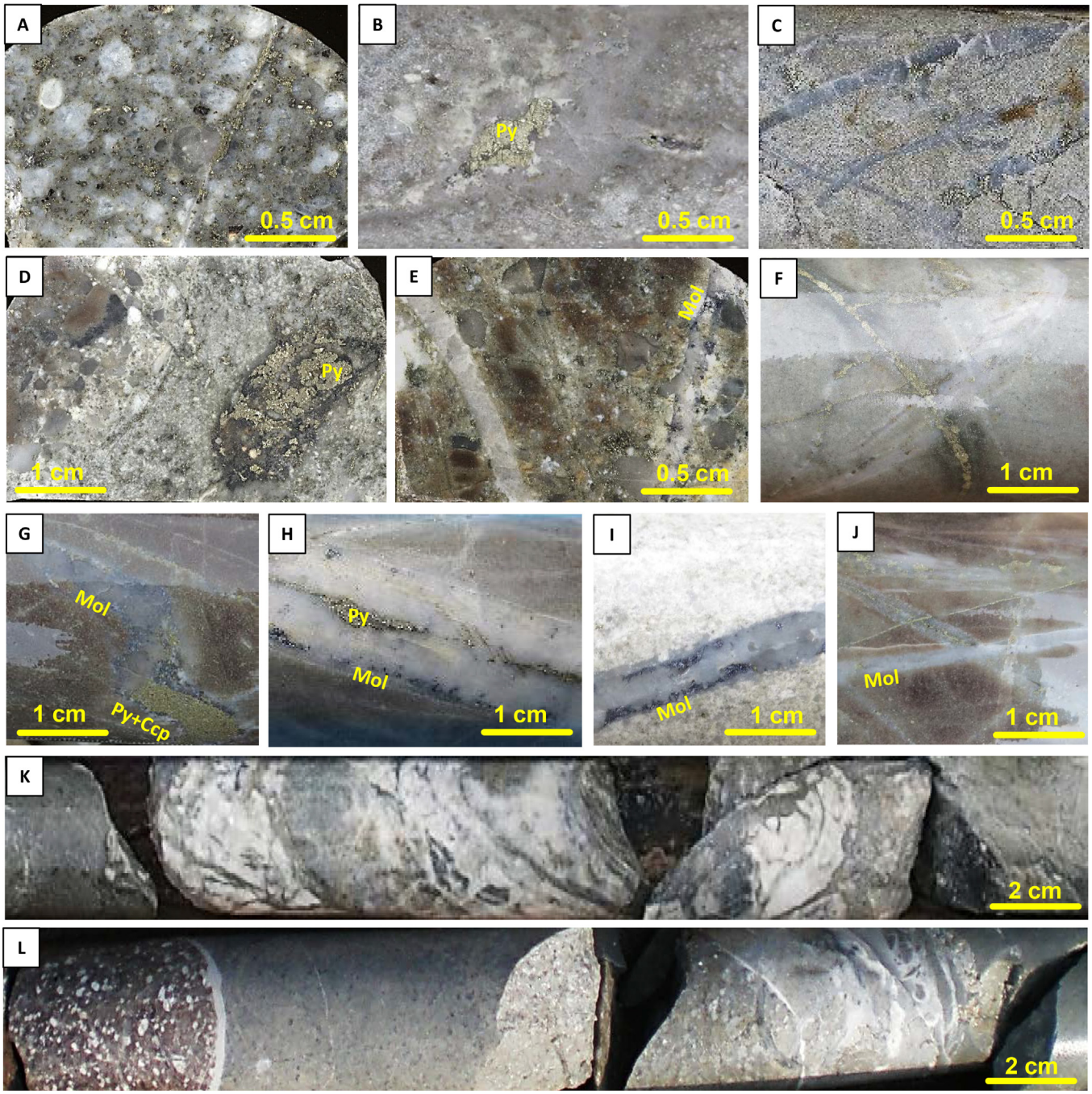

Fig. 9. Photographs showing some typical features of phyllic alteration assemblages and late quartz-sulfide veins in the Lazurnoe deposit area. A. Granodiorite-porphyry is overprinted by phyllic alteration (Srednee Zone; polished slab). B. Granodiorite-porphyry is almost entirely replaced by phyllic alteration (Srednee Zone; polished slab). C. Zone of intense (almost entire) silicification to quartz-sericite alteration ("quartz core"), with quartz-pyrite veinlets, related to phyllic alteration (Srednee Zone; polished slab). D. Hydrothermal breccia with quartz-sericite-pyrite matrix contains fragments of chlorite-magnetite-pyrite aggregate of propylitic alteration (Srednee Zone; polished slab). E. Magmatic breccia with quartz monzonite- to granodiorite-porphyry matrix cementing fragments of chert, biotite hornfels, and quartz is cut by quartz-pyrite and quartz-molybdenite veinlets of phyllic alteration (Srednee Zone; polished slab). F. Barren quartz veinlet is cut by quartz-pyrite veinlet in zone of quartz-sericite replacement of potassic (biotite-quartz) alteration (Srednee Zone; drill core). G. Quartz-pyrite-chalcopyrite-molybdenite veinlet with sericitic selvages cutting zone of pervasive potassic (biotite-quartz) replacement (Lazurnoe Zone; drill core). H. Quartz-pyrite-molybdenite veinlet the central pyrite "line" and sericitic selvages cutting zone of pervasive potassic alteration (Lazurnoe Zone; drill core). I. Quartz-molybdenite veinlet in zone of pervasive quartz-sericite alteration. (Lazurnoe Zone; drill core). J. Quartz-pyrite veinlet with a central pyrite "line" is cut by quartz-molybdenite veinlet, both cutting zone of pervasive potassic alteration (Srednee Zone; drill core). K-L. Late quartz-carbonate-sericite-sulfide veins with arsenopyrite, pyrrhotite, pyrite and chalcopyrite (Lazurnoe Zone; drill core). Abbreviations: Py – pyrite, Mol – molybdenite.

inclusions and densities for the low-density fluid inclusions (e.g., Roedder, 1984). The densities of carbonic phases, containing CH_4 in addition to CO_2, can be determined by diagrams from Thiery et al. (1994), using final CO_2 melting and carbonic phase homogenization temperatures measured. On this basis, and using the computing programs of Bakker (2003), the pressure of ~550 ± 50 bars at the temperature of 340–380 °C has been obtained. This pressure corresponds to a depth of ~2.2 km assuming lithostatic conditions (cf. Fournier, 1999).

Table 3
Types of fluid inclusions (FI) in minerals from various hydrothermal assemblages of the Lazurnoe deposit.

Mineral (number of FI measured)	FI type	FI size	FI content	T_m eu., °C	T_m CO_2, °C	T_m ice, °C	T_h carb, °C	T_m clathrate, °C	Mode and temperature of final homogenization, T_h, °C	Estimated salinity, wt.% NaCl-eq.	Estimated CO_2/CH_4 ratio[e]	Estimated pressure, bars, (T_h correction)
Quartz-K-feldspar to quartz-biotite veinlets (potassic alteration)												
Quartz (20)	1	5–30 μm	Multisolid, with halite and 3–4 anisotropic to opaque solids, 20–25 vol% gas	−65		−30…–33			Gas to liquid at 350–380, halite to liquid at 430–455	NaCl 45–48 [a]$CaCl_2$ 10–9 [a]		> 850[d](> 80)
Quartz-chlorite-sulfide veinlets (propylitic alteration)												
Quartz (18)	2–1	5–30 μm	Multisolid, with halite and 1–2 anisotropic to opaque solids, 10–15 vol% gas	−65		−50…-48			Gas to liquid at 280–310, halite to liquid at 325–335	NaCl 29–31 [a]$CaCl_2$ 19–18 [a]		> 400[d](. > 40)
Quartz (11)	2–2	5–20 μm	Multisolid, with halite and 1–2 anisotropic to opaque solids, 10–15 vol% gas	−65		−35…–33			Gas to liquid at 280–310, halite to liquid at 250–260	NaCl 24–25 [a]$CaCl_2$ 17–16 [a]		(. > 40)
Quartz (30)	2–3	5–20 μm	Liquid-gaseous with 0–1 opaque solid, 20–25 vol% gas	−60		−25…-24			Gas to liquid at 280–310	NaCl 12 ± 0.5 [a]$CaCl_2$ 12 ± 0.5[a]		(. > 40)
Quartz-sericite to quartz-sericite-sulfide veinlets (phyllic alteration)												
Quartz (15)	3	5–30 μm	Multisolid, with halite and occasional 0–4 anisotropic to opaque solids, 10–15 vol% gas	−55		–23…–22			Gas to liquid at 150–230, halite to liquid at 230–310	NaCl 30–37 [a]$CaCl_2$ 5 ± 0.5 [a]		> 850[d](> 80)
Auriferous quartz-carbonate-sericite-sulfide veins ("late quartz-sulfide veins")												
Quartz (20)	4A	5–30 μm	90–95 vol% gas		−59.5 to −58.5		17 to 19 to gas	7.5 to 8.5	Liquid to gas at 350–390	3-5[c]	85:15	550 ± 50[f]
Quartz (16)	4B	5–30 μm	40–50 vol% gas	−29 to −25		−6.5 to −4.5		4.5 to 5.5	Gas to liquid at 340–380	7.2–9.9[b,c]		
Quartz (21)	5	5–15 μm	20–25 vol% gas	−27.5 to −26.5		−7.3 to −3.5			Gas to liquid at 250–295	5.7–10.9[b]		

T_m eu. – eutectic temperature (first ice melting temperature), °C; T_m CO_2 – final CO_2 melting temperature, °C; T_m – final ice melting temperature, °C; T_h carb – carbonic phase liquid to gas homogenization temperature, °C; T_m clathrate – clathrate melting temperature, °C.

[a] Salinity was estimated by halite dissolution temperature and final ice/hydrohalite melting temperatures for the NaCl-$CaCl_2$-H_2O system (Vanko et al., 1988; Oakes et al., 1990).

[b] Salinity was estimated by final ice melting temperature (Bodnar and Vityk, 1994).

[c] Salinity was estimated by clathrate melting temperature (Darling, 1991).

[d] The minimal trapping pressure was estimated by using the T_h and halite melting temperature (Atkinson, 2002; Becker et al., 2008).

[e] The ratio was estimated by final CO_2 melting and carbonic phase homogenization temperatures (Thiery et al.,1994).

[f] The pressure was estimated by using the T_h of type B fluid inclusions and the density of type A fluid inclusions trapped contemporaneously (Bakker, 2003).

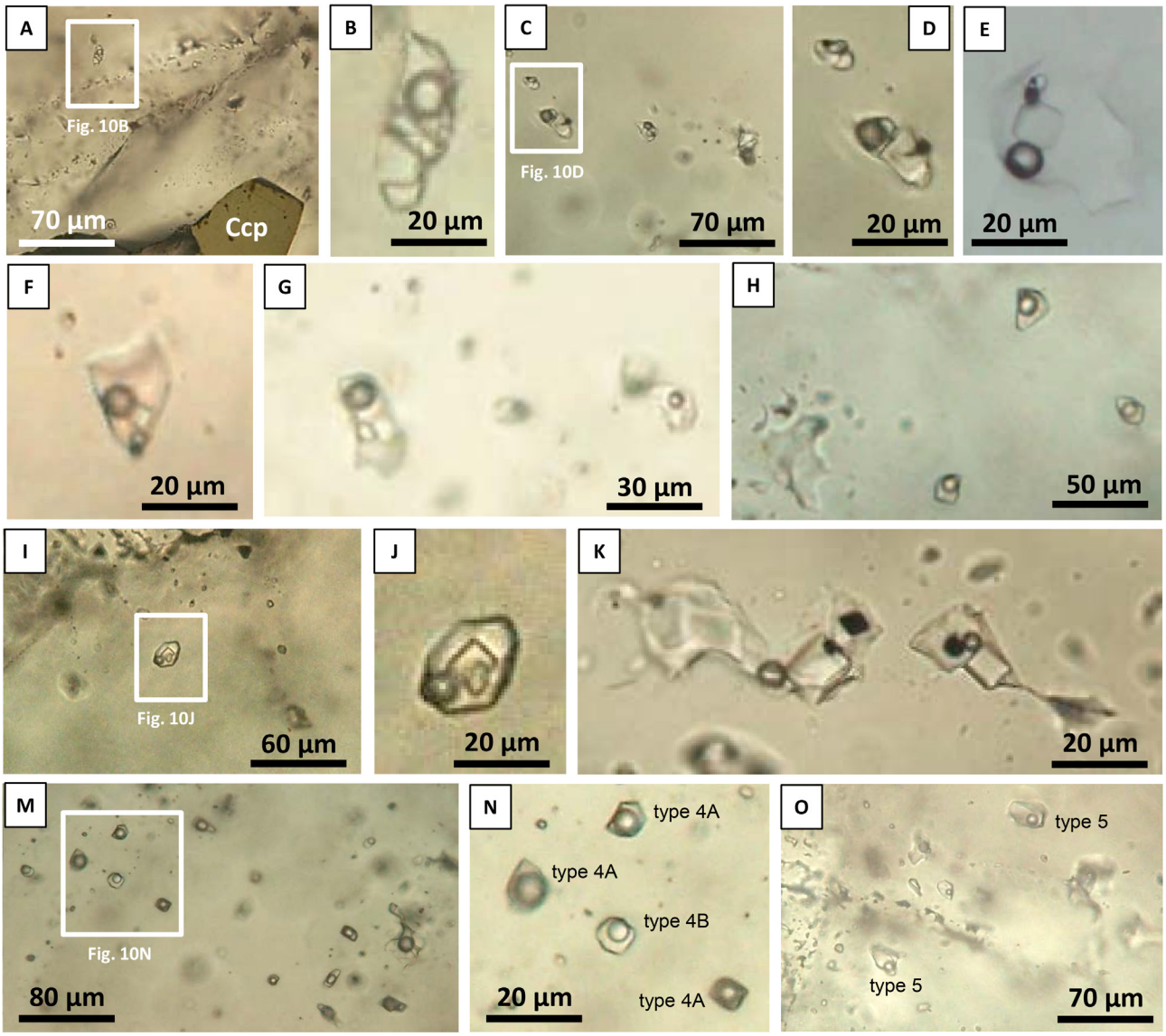

Fig. 10. Types of fluid inclusions in minerals from various hydrothermal alteration assemblages at the Lazurnoe deposit. A-D. Multisolid type 1 fluid inclusions in quartz from potassic alteration assemblage (B, D – larger views) (Cct – chalcopyrite). E-F. Multisolid type 2–1 fluid inclusions in quartz from propylitic alteration assemblage. G. Multisolid type 2–2 fluid inclusions in quartz from propylitic alteration assemblage. H. Gaseous-liquid type 2–3 fluid inclusions in quartz from propylitic alteration assemblage. I-K. Multisolid type 3 fluid inclusions in quartz from phyllic alteration assemblage (J – larger view; K – type 3 inclusions with possible post-entrapment modification causing the inclusion "salting out" that supports their high and variable, in terms of a number of dissolved species, salinity). M-N. Coexisting type 4A gaseous and type 4B liquid-gaseous fluid inclusions in quartz from the late quartz-carbonate-sulfide veins (N – larger view). O. Liquid-gaseous type 5 fluid inclusions in quartz from the late quartz-carbonate-sulfide veins.

Due to boiling, no pressure correction is necessary for the homogenization temperature of 340–390 °C.

9. Sulfur isotope analysis

The sulfur isotope data (Table 4) displays homogenous sulfur isotope values, with $\delta^{34}S$ values being close to the meteorite standard. However, sulfides from every hydrothermal alteration type range from negative to positive $\delta^{34}S$ values, i.e., $\delta^{34}S$ values range from −1.6 to +2.2‰ in chalcopyrite and pyrite from potassic alteration assemblages, from −1.5 to +3.2‰ in chalcopyrite and pyrite from propylitic alteration assemblages, and from −3.0 to +2.9‰ in chalcopyrite and pyrite from phyllic alteration assemblages. In contrast, pyrite, chalcopyrite, pyrrhotite and arsenopyrite from the late auriferous quartz-sulfide veins show more consistent enrichment in heavy sulfur isotope illustrated by $\delta^{34}S$ values ranging from +1.6 to +3.4‰ (Table 4).

10. Discussion

10.1. Tectonic setting and magmatic sources

The Lazurnoe deposit is an important emerging porphyry Cu-Au-Mo deposit in the Sikhote-Alin associated with high-K calc-alkaline to shoshonitic magmatism and specifically to that occurred in a continental transform margin setting after the cessation of active subduction. As emphasized by Khanchuk et al. (2016), Grebennikov et al. (2016) and other authors, subduction in the region was terminated before the continental transform regime commenced in the Hauterivian (~145 Ma) and continued until subduction resumed in the Late Cretaceous (principally post-Cenomanian; ~95 Ma). This period is subdivided into three stages, namely, (1) a stage of intense strike-slip displacement and deformation of the Jurassic and Early Cretaceous terranes, with the initiation of turbidite basins, during the Hauterivian-

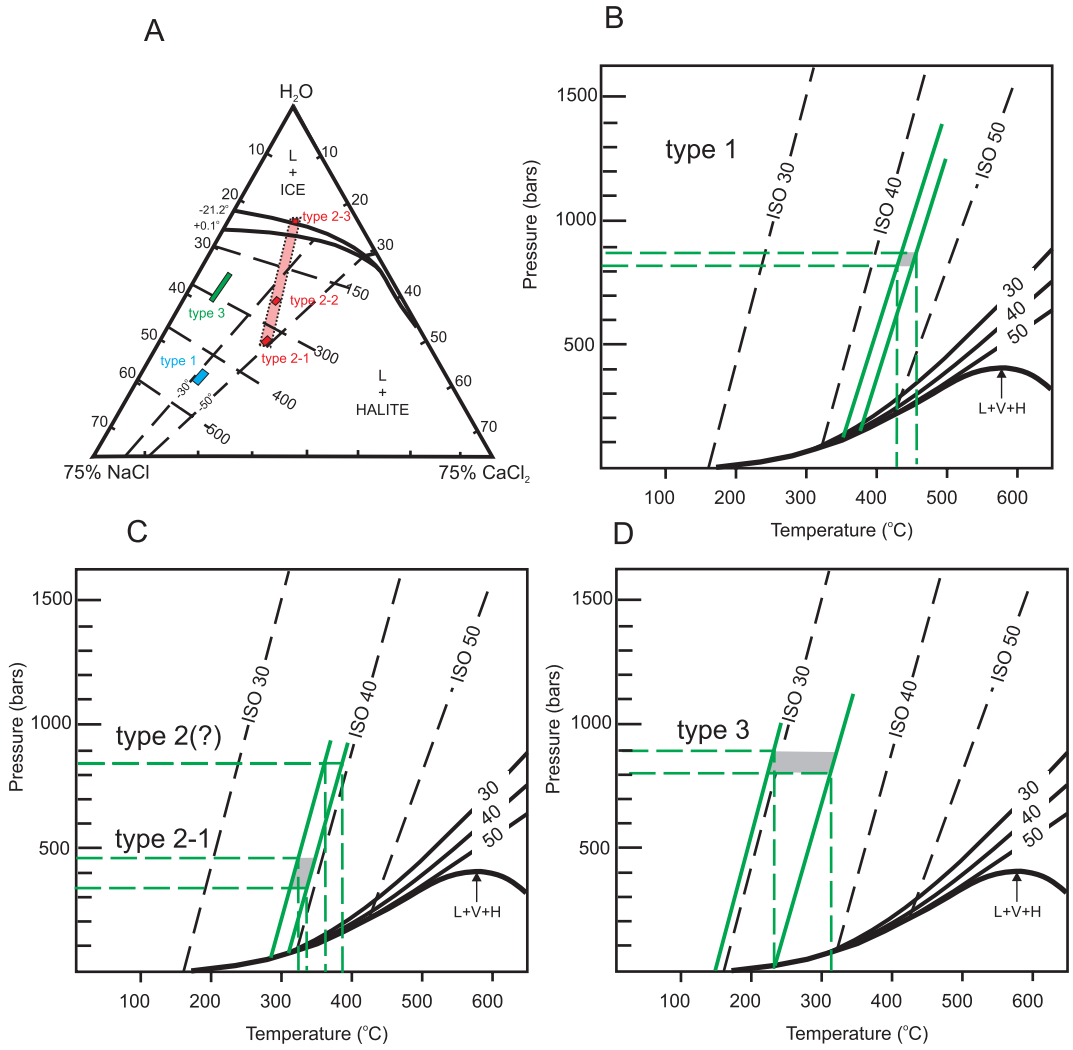

Fig. 11. A. Diagram showing the composition of the type 1, 2 and 3 fluid inclusions in the NaCl-$CaCl_2$-H_2O system (after Vanco et al., 1988; Oakes et al., 1990). B-D. Minimum pressure (shaded area) estimates for the entrapment of the type 1, 2 and 3 fluid inclusions in minerals from potassic alteration (B), propylitic alteration (C) and phyllic alteration (D) assemblages. Vapor-pressure curves for H_2O-NaCl solutions and isochors (labelled in wt.% NaCl) as well as the three-phase (L + V + H) curve for the NaCl-H_2O system are from Atkinson (2002), Becker et al. (2008) and correspond to most common salinities of halite-bearing fluid inclusions determined in this study (30–50 wt% NaCl-equiv., respectively).

Aptian (145–125 Ma), (2) a stage of a continent-arc collision in the late Aptian-early Albian (125–115 Ma), when the development of the turbidite basins continued, combined with a *syn*-strike-slip compression caused by a collision with an Early Cretaceous island arc, and (3) a stage of further development of the transform margin during the late Albian-early Cenomanian (115–95 Ma). During the first and the third stages, the subducted slab break-off occurred, with corresponding asthenospheric mantle upwelling and injection through the slab windows; this resulted in the intrusion of granitoids with mixed crustal-mantle geochemical signatures and intrusions of a shoshonitic magma (Kruk et al., 2014; Jahn et al., 2015; Khanchuk et al., 2016). The latter, at the Lazurnoe deposit, are dated at ~100 Ma, thus falling within the late Albian-early Cenomanian stage of the transform margin development. Similar to the W-Au-Sn metallogenic belt, the Lazurnoe deposit area is aligned with the Central Sikhote-Alin strike-slip fault.

By its tectonic setting affected by a strike-slip regime occurring at a continental transform margin after the cessation of active subduction, the Lazurnoe deposit exhibits distinct similarities to some other porphyry Cu-Au-Mo deposits situated in the northern Pacific region. In particular, the formation of the giant Pebble porphyry Cu-Au-Mo deposit in Alaska broadly overlapped the cessation of sedimentation and contraction and the transition to a transpressional continental margin regime, with the conversion of the remnant ocean basins to strike-slip basins (Goldfarb et al., 2013). Magmatic activity followed lithosphere thickening and an asthenospheric mantle upwelling, with subsequent post-subduction partial melting of the subcontinental lithospheric mantle and the intrusion of shoshonitic magma to shallow levels (Lang et al., 2013).

The post-subduction setting of Lazurnoe and its possible relationship with asthenospheric mantle upwelling provides also similarities to the copper-porphyry deposits formed in collisional tectonic settings (e.g., Hou and Cook, 2009; Hou et al., 2003, 2009, 2011; Ludington et al., 2012; Yang et al., 2016). In particular, in the Tibet-Himalayan orogen, similar assemblages of igneous suites and related mineralization were formed during collision-related tectonic stages including (1) the main stage of convergent collision, (2) stage of late-collisional transform continental margin, and (3) stage of post-collisional extension (Hou and Cook, 2009; Ludington et al., 2012). During the collision stage, the sequence of igneous suites and related metallogenic types included ilmenite-series granitoids accompanied by Sn-W deposits and orogenic Au deposits. During the stage of transform continental margin, Au-Mo-Cu porphyry deposits related to shoshonitic suites were formed (Hou and Cook, 2009; Ludington et al., 2012). Further evolution toward post-collisional extension has resulted in the intrusions of younger

Table 4
Sulfur isotope compositions of sulfide minerals from the Lazurnoe deposit area.

Samples	Description	Ccp	Py	Po	Apy
		$\delta^{34}S_{VCDT}$, ‰			
Potassic alteration					
DC5-44.1	Quartz-K-feldspar alteration with chalcopyrite and trace to minor magnetite	−1.3			
DK-105-217	Quartz-K-feldspar alteration with chalcopyrite and trace to minor magnetite	−1.1			
LC7-52	Quartz-K-feldspar alteration with chalcopyrite and trace to minor magnetite	−1.6			
DC4-93.4	Quartz-K-feldspar veinlet with chalcopyrite and pyrite	+0.1	−1.3		
DC5-126	Quartz-K-feldspar veinlet with chalcopyrite	+2.2			
Propylitic alteration					
LC7-64	Quartz-chlorite alteration with chalcopyrite and pyrite	−1.5			
LC7-92	Quartz-chlorite alteration with pyrite and chalcopyrite	−1.1			
LC9-33.5	Quartz-chlorite alteration with chalcopyrite and pyrite	−1.5			
LC9-134	Quartz-chlorite alteration with chalcopyrite and pyrite	−1.0			
DC-104-66.6	Quartz-chlorite alteration with pyrite and chalcopyrite	−0.1			
S1-198.4	Disseminated pyrite from propylitic alteration with chalcopyrite		+2.2		
S2-106.2	Quartz-chlorite alteration with chalcopyrite and pyrite		+2.1		
S2-144.5	Quartz-chlorite alteration with chalcopyrite and pyrite		+3.0		
LK-308-260	Pyrite with inclusions of epidote, albite, quartz in propylitic alteration zone with magnetite		+3.2		
Phyllic alteration					
LK-302-174.5	Semi-massive chalcopyrite from quartz-chalcopyrite veinlet	−1.3			
LC6-125.4	Quartz-chalcopyrite-pyrite-molybdenite veinlets intersecting propylitic zone with magnetite	−1.5			
LC6-170.2	Quartz-sericite veinlets with pyrite, chalcopyrite and molybdenite	−1.9			
LC6-179.6	Quartz-sericite alteration with pyrite and chalcopyrite		−3.0		
LC9-183	Quartz-sericite alteration with pyrite and chalcopyrite	−1.5			
LK-313-122.5	Thick quartz veinlet with chalcopyrite and pyrite	+0.1			
L-2008-1	Pyrite dissemination and veinlets with minor chalcopyrite		+2.6		
S1-97	Quartz-sericite alteration with pyrite and chalcopyrite overprinting propylitic alteration		+1.2		
S2-54.7	Quartz-sericite alteration with pyrite, chalcopyrite and molybdenite		+2.9		
Late auriferous quartz-sulfide veins					
LC6-67.1	Quartz-sericite-carbonate alteration with chalcopyrite, pyrite and galena	+2.4			
LC6-234	Quartz-sericite-carbonate vein with chalcopyrite, pyrite and pyrrhotite	+2.1			
LK-305-4.5	Quartz-sericite alteration with chalcopyrite, pyrite and pyrrhotite overprinting propylitic alteration	+3.4			
LK-302-251	Disseminated chalcopyrite, pyrrhotite and pyrite overprinting propylitic alteration			+2.6	
LK-313-210.5	Disseminated pyrrhotite and chalcopyrite overprinting propylitic alteration		+2.8		
L-2007-3	Thick quartz vein with pyrite, pyrrhotite and arsenopyrite			+3.0	
L-2085	Quartz-pyrite veinlets accompanying thick quartz-pyrrhotite-arsenopyrite-chalcopyrite-pyrite vein				+1.6
S1-243.9	Quartz-sericite-carbonate vein with chalcopyrite, pyrite and pyrrhotite		+1.8	+1.9	
S1-278.1	Disseminated chalcopyrite, pyrrhotite and pyrite		+2.0		

Abbreviations: Ccp – chalcopyrite, Py – pyrite, Po – pyrrhotite, Apy – arsenopyrite.

shoshonitic suites and formation of Sn-polymetallic deposits, thus further highlighting a common formation of both porphyry Cu-Au-Mo and Sn-polymetallic deposits in the post-subduction environments (e.g., Gonevchuk et al., 2005, 2010; Soloviev, 2014).

There are significant differences in conditions of magma generation and magmatic sources of shoshonitic igneous suites forming, respectively, in subduction-related and post-subduction settings (Richards, 2009, 2011a; Guo et al., 2006; Ludington et al., 2012; Soloviev, 2014; Muller and Groves, 2019). In particular, fertile porphyry intrusions in subduction-related settings are linked to magmatic sources in the lithospheric mantle and/or at the mantle/crust boundary (e.g., Richards, 2009, 2011a; Garwin et al., 2005). In contrast, for the post-subduction settings, Richards (2009, 2011a) suggested re-melting of earlier subducted lithosphere comprising amphibolite cumulates and containing small amounts of sulfide minerals concentrating chalcophile and siderophile elements; this process could produce oxidized magmas with a high water content. Hou et al. (2011) suggested a model implying partial melting of thickened or delaminated lower crust of mafic composition containing components of asthenospheric mantle, whereas productivity of the generated magma depends on Cu and Au supply from mantle and lower crust that were metasomatized during subduction and accumulation of mafic melts in the lower crust. These processes occurring at the post-subduction stages are facilitated by asthenospheric mantle ascent through a slab window formed in the subducted slab, or by that caused by lithosphere delamination. Pirajno (2010) emphasized the role of large strike-slip fault zones in the decompression melting of the mantle material, with the generation of mafic magmas and their emplacement along the comparatively narrow conduits of the strike-slip zones. This process was feasible in the zone of the Central Sikhote-Alin fault and could further contribute to the generation of fertile porphyry magmas (cf. Hou et al., 2003). Zhou et al. (2019) suggested that high-Sr/Y shoshonites can be produced by partial melting of juvenile lower crust affected by ultrapotassic or potassic mafic magmas, whereas fertile (with respect to Cu-Au-Mo mineralization) high-Sr/Y shoshonitic magma is formed if this partial melting is intensely water-fluxed.

Geochemical signatures of the Lazurnoe suite igneous rocks, such as elevated Nb, Ta, Zr and Pb contents (Fig. 5J), suggest the magma sourcing from a subduction-modified mantle (e.g., Pearce et al., 1984), thus confirming an early subduction event and subsequent remelting of the subcontinental lithosphere in a post-subduction environment. Commonly for shoshonitic series (e.g., Wallace and Carmichael, 1992; Zhang et al., 2008; Muller and Groves, 2019), the initial (mafic) magma generation at Lazurnoe could be related to a low degree of partial melting (~2.5–3 vol%; Fig. 12A and B) of a metasomatized K-rich lithospheric mantle, such as amphibole-spinel to amphibole-garnet peridotite, phlogopite-garnet peridotite, or garnet-spinel lherzolite. Progressive mantle magma source enrichment continued during the magma generation (Fig. 12C), thus contributing to the replenishment of magmatic reservoir to form younger intrusive phases. Alternatively, the positive Zr and Pb anomalies are consistent with an addition of crustal-derived magma (Pearce and Peate, 1995); the crustal geochemical

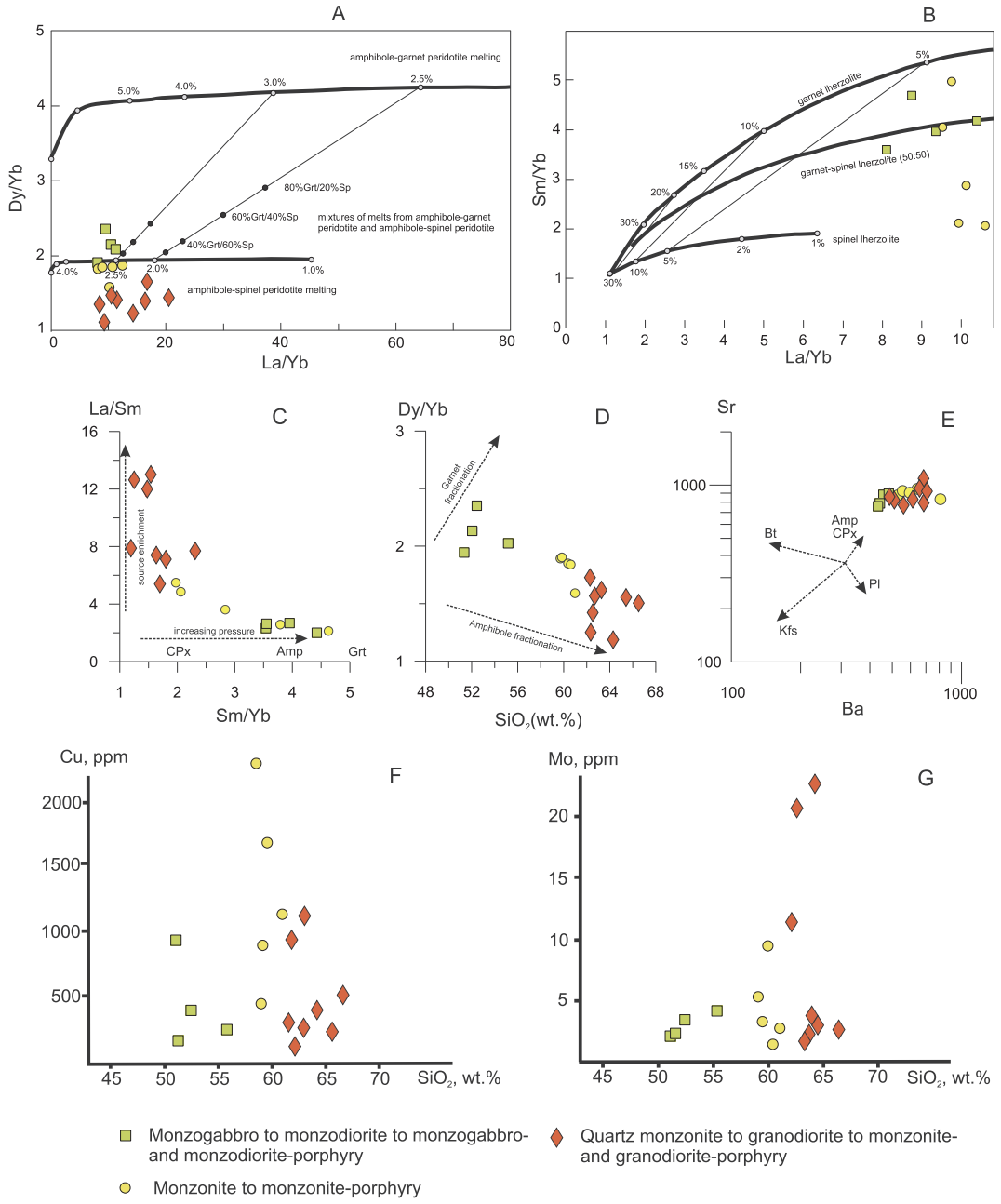

Fig. 12. Geochemical diagrams showing conditions of magma generation and evolution of the Lazurnoe plutonic suite. (A) Dy/Yb vs. La/Yb diagram showing compositional fields of mafic alkaline magmas generated under amphibole-garnet and amphibole-spinel peridotite melting, with the respective proportions of mixing between these melts (Jung et al., 2006). Numbers on model curves indicate the percent melting. Points at 80Grt/20Sp, 60Grt/40Sp and 40Grt/60Sp indicate mixing proportions of melts from amphibole-garnet peridotite (e.g., 80 vol%) with melts from amphibole-spinel peridotite (e.g., 20 vol%). Note that the stage 3 rock compositions plot outside the model fields, thus indicating the incompatibility of these rock compositions to a mantle source. (B) Sm/Yb vs. La/Yb diagram showing compositional fields of mafic alkaline magmas generated under garnet to spinel lherzorite melting (Zhao and Zhou, 2009). Numbers on model curves indicate the percent melting. Note that the stage 3 and partially stage 2 rock compositions plot outside the model fields, thus indicating the incompatibility of these rock compositions to a mantle source. (C) La/Sm vs. Sm/Yb diagram displaying approximate stability thresholds of clinopyroxene, amphibole and garnet stabilities in mantle melt residues (Moritz et al., 2016). (D) Dy/Yb vs. SiO_2 diagram displaying amphibole and garnet fractionation trends (Davidson et al., 2007). (E) Sr vs. Ba diagram showing dominant trends of crystallization differentiation. (F-G) Distribution of Cu (F) and Mo (G) in the igneous rocks. Abbreviations: CPx – clinopyroxene, Amp – amphibole, Grt – garnet, Bt – biotite, Pl – plagioclase, Ksp – K-feldspar. The individual rock compositions are from Table 2.

signatures become stronger in the younger (2nd and particularly 3rd stage) rocks. The latter is consistent with a model implying generation, under the influence of mantle-supplied fluids and heat, granitic magmas in the crustal protolith, with further mixing/mingling of the mantle-related mafic (shoshonitic) magma and mantle-induced crustal granitic magma. Mixing/mingling of compositionally contrasting magmas is supported by the presence of embayed quartz phenocrysts in quartz monzonite and granodiorite at Lazurnoe (cf. Hibbard, 1995). The decreasing pressure of magma generation (Fig. 12C) may be indicative of a shallower pressure magma differentiation due to thinning/extension of the crust (cf. Moritz et al., 2016).

10.2. Magma fractionation

The high-K calc-alkaline to shoshonitic rocks of the Lazurnoe plutonic suite evolved toward water saturation that was favored by intense

amphibole fractionation; the latter is consistent with negative correlation between Dy/Yb ratios and increasing SiO_2 contents (Fig. 12D; Davidson et al., 2007; Moritz et al., 2016). The role of plagioclase fractionation was relatively minor during the 1st and 2nd intrusive stages (consistent with the lack of Eu anomalies) and slightly increased, together with biotite and K-feldspar fractionation, at the 3rd intrusive stage (Fig. 12E). Consistent with the decompression-driven crystallization and cooling (cf. Rezeau et al., 2018), and together with dominant amphibole fractionation reflecting a high magmatic water content, this provided some adakitic signatures of the 3rd stage igneous rocks at Lazurnoe (cf. Moritz et al., 2016). As emphasized by Richards (2011b), presence of hydrous phenocryst phases (amphibole, biotite) indicating increasing magmatic water content, with abundant amphibole fractionation but suppressed plagioclase crystallization at deep crustal levels, together with high oxidation states and elevated sulfur content, positively affects magma fertility for Cu-Au mineralization.

Sulfide saturation necessary to produce Cu mineralization associated with porphyry intrusions is limited in the oxidized (magnetite-series) magma and occurs after magnetite fractionation. The latter occurring at ~60 wt% SiO_2 triggers sulfide saturation due to the conversion of most of the sulfur originally dissolved in the magma as sulfate, with the Cu-rich sulfide phase represented by bornite sequestering gold (Jenner et al., 2010). Sun et al. (2015) emphasized that the oxidized magma remains sulfide-undersaturated during the early stages of its evolution; sulfide saturation occurs and the metals are partitioned into coexisting magmatic-hydrothermal fluids following reduction accompanying magnetite crystallization. Consistently, Cu distribution in the igneous rocks at Lazurnoe shows a tendency of enrichment during the 1st and 2nd intrusive stages, with the metal contents generally dropping as magmatic differentiation progresses during the 3rd intrusive stage (Fig. 12F). The highest Mo contents occur in the more differentiated 3rd stage rocks (Fig. 12G) suggesting a decoupling of these elements during the magmatic-hydrothermal evolution, with Mo transition into hydrothermal-magmatic fluids at younger stages.

10.3. Alkalic porphyry Cu-Au-Mo deposit model

The association of Lazurnoe with high-K calc-alkaline to shoshonitic igneous suite allows its classification toward the group of alkalic, shoshonite-related porphyry Cu-Au-Mo deposits (Muller and Groves, 2019; Cooke et al., 2007; Bissig and Cooke, 2014, and references therein). More specifically, it can be assigned to the "silica-saturated" subtype (Lang et al., 1993) due to ubiquitous quartz in hydrothermal alteration assemblages as well as lack of silica-deficient minerals in the parental igneous rocks. This is consistent with some other features of such systems at Lazurnoe including (1) limited development to lack of the most acidic (argillic, etc.) alteration types (e.g., Holliday and Cooke, 2007), (2) stronger development of calcic (calc-potassic, calcic-sodic) assemblages comprising calcite, amphibole, epidote, (3) greater role of magmatic-hydrothermal Ca-rich fluids (Sillitoe, 2010), (4) greater abundance of magnetite (Holliday and Cooke, 2007), (5) presence of PGE mineralization (Bissig and Cooke, 2014). These signatures can be accounted to establish a group of alkalic porphyry Cu-Au-Mo deposits formed in the continental transform margin settings (e.g., Muller and Groves, 2019).

10.4. Magmatic-hydrothermal fluid evolution

Similar to other shoshonite-related magmatic-hydrothermal systems (e.g., Richards, 1995; Muller and Groves, 2019), a combination of a deep-rooted (likely mantle-related) magmatic source with a shallow crustal level of magma emplacement and degassing is suggested at Lazurnoe. Magma emplacement at shallow levels promotes direct exsolution of metalliferous high-salinity aqueous fluids from crystallizing volatile-rich intrusions (Cline and Bodnar, 1994; Bodnar, 1995; Shinohara and Hedenquist, 1997; Harris et al., 2004; Audetat et al., 2008). These high-salinity fluids could be parts of more complex fluids evolution, as the exsolved fluids exhibit either a decreasing salinity trend while exsolving from magmas crystallized at a relatively greater depth, or an increasing salinity trend while exsolving from magmas crystallized at shallower depths (e.g., Audetat et al., 2008).

The model implying a direct exsolution of high-salinity aqueous fluids from crystallizing magma would be consistent with the presence of type 1, 2 and 3 fluid inclusions in various hydrothermal assemblages at Lazurnoe. In particular, potassic alteration assemblages were formed from a homogenous carbonic-free, hot (~530–510 °C), high-salinity (45–48 wt% NaCl and 9–10 wt% $CaCl_2$), calcic-sodic aqueous-chloride type 1 fluid inclusions in minerals of potassic alteration assemblages at Lazurnoe (Table 3). Propylitic alteration assemblages were formed from a cooler (< 450–400 °C), more diluted, homogenous calcic-sodic aqueous-chloride fluid (type 2 inclusions) that was characterized by decreasing salinity (from 29 to 31 wt% NaCl and 18–19 wt% $CaCl_2$ through 24–25 wt% NaCl and 16–17 wt% $CaCl_2$ to 12 ± 0.5 wt% NaCl and 12 ± 0.5 wt% $CaCl_2$) (Table 3). This fluid evolution likely corresponds to a continuous exsolution of magmatic-hydrothermal fluid from crystallizing magma, with decreasing fluid salinities under similar temperatures and pressures (Fig. 11A; Table 3). Pressure estimates (850 ± 50 bars) obtained for type 1 and 2 fluid inclusions in potassic and propylitic alteration minerals correspond to depths of about 3.5 km assuming lithostatic conditions (Fig. 13; cf. Fournier, 1999). These or slightly shallower depth estimates are consistent with the development of magmatic crystallization porphyry textures in the igneous rocks.

In contrast, another cycle of fluid exsolution from crystallizing magma can be suggested for phyllic alteration assemblages (Fig. 13; cf. Harris and Golding, 2002) that were formed from a homogenous high-salinity (30–37 wt% NaCl and 5 ± 0.5 wt% $CaCl_2$) calcic-sodic aqueous-chloride fluid (type 3 inclusions; Table 3). The cyclic release of magmatic-hydrothermal fluid from crystallizing magma could be due to periodical fluid-melt recharging events, with subsequent periodic refertilization of volatiles linked with source pluton evolution (Li et al., 2017a,b; Williamson et al., 2016). On the other hand, the type 3 fluid inclusion homogenization temperatures (~390–310 °C) appear to be too low to establish a direct link to a magma and may indicate that the fluids were separated at depth and cooled before reaching the mineral deposition level. No boiling recorded at either hydrothermal stages of the "porphyry cycle" at Lazurnoe, and this is in contrast to many Cu-Au-Mo porphyry deposits (e.g., Cooke et al., 2005; Sillitoe, 2010; Kouzmanov and Pokrovski, 2012).

The dominant association of productive Cu-sulfide mineralization with zones of potassic alteration, particularly with quartz-K-feldspar and quartz-K-feldspar-biotite veinlets, which formed at ~530–510 °C (Table 3), indicates a relatively high-temperature mineralization. This is similar to many porphyry Cu-Au-Mo deposits, where Cu and Au are precipitated mainly at the potassic alteration stage (e.g., Lowell and Guilbert, 1970; Seedorff et al., 2005; Sillitoe, 2010). However, this is in contrast to the other porphyry Cu-Au-Mo deposits, where Cu is paragenetically late (e.g., Pirajno, 2009) and where the main Cu-ore deposition occurred in the porphyry environment at lower temperatures, in the order of 350–300 °C and lower (e.g., Hedenquist et al., 1998; Harris and Golding, 2002; Harris et al., 2004; Seedorff et al., 2005; Rusk et al., 2008; Klemm et al., 2007; Gregory, 2017; Tsuruoka, 2017). The dominant association of Cu mineralization with potassic alteration, with a minor input from later mineralizing processes during the propylitic and phyllic alteration stages, can further explain the relatively low Cu and Au grades at Lazurnoe. Notably, the Cu grades are remarkably higher in local intervals of propylitic alteration overprinting potassic alteration (Fig. 3). Instead, Mo mineralization at Lazurnoe formed mostly during the younger phyllic stage and correspondingly at lower temperatures (~390–310 °C).

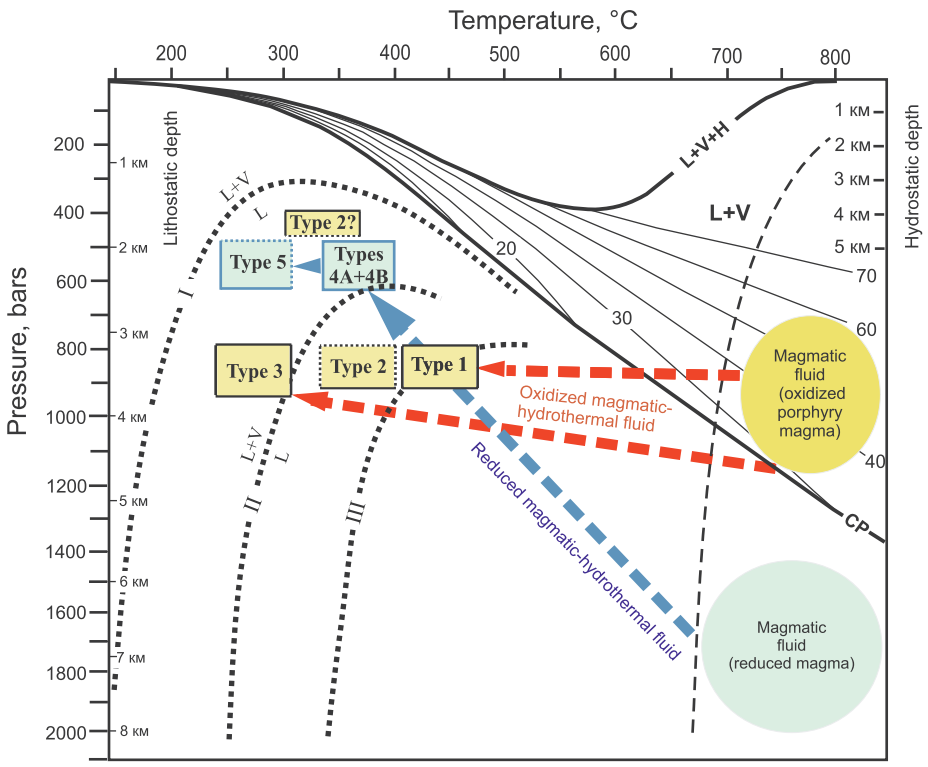

Fig. 13. Estimated pressure and temperature conditions and evolutional paths for different fluid inclusion types in hydrothermal assemblages at the Lazurnoe deposit, with composition of different fluid inclusion types as a function of depth and temperature (the principal diagram after Bodnar et al., 1985; Fournier, 1999). Vapor-pressure curves for H_2O-NaCl solutions at 0–70 wt% NaCl-eq. and the three-phase (L + V + H) curve are shown after Atkinson (2002) and Becker et al. (2008). Dashed line represents water-saturated granite solidus (Holtz et al., 2001). The two-phase (L/L + V) curves (dotted lines) for H_2O-NaCl-CO_2 fluid containing 6 wt% NaCl and 4.08 mol.% CO_2 (curve I), 10 mol.% CO_2 (curve II), and 21.33 mol.% CO_2 (curve III) (Schmidt and Bodnar, 2000) are presented. PT-fields for the major fluid inclusion types and possible evolutional paths for fluids (arrows) are shown.

10.5. Late auriferous quartz-sulfide veins: reduced intrusion-related Au model?

Origin of the late auriferous quartz-sulfide veins remains controversial, as their mineral composition, with abundant arsenopyrite and pyrrhotite, together with pyrite, native Au and locally sphalerite and galena, indicates a reduced environment, in contrast to the preceding oxidized, magnetite-stable potassic, propylitic and phyllic alteration assemblages. A similar evolution from magnetite- to pyrrhotite (± arsenopyrite)-stable conditions was reported in many other porphyry (to skarn) Cu-Au-Mo systems (e.g., Seedorff et al., 2005), with the late-stage fluid and metal supply possibly occurring from residual mafic magma chambers (e.g., Soloviev et al., 2018).

However, structural setting of these veins is sharply different from that of the porphyry-style mineralization indicating their relationships to larger faults rather than to local “porphyry centers”. In addition, the presence of carbonic-rich fluid inclusions containing methane is also in contrast to “porphyry type” fluids at Lazurnoe lacking carbonic phase (s). As noted by Baker (2002), CO_2 is exsolved from magma at much deeper levels than those of Cu-porphyry intrusion crystallization; this is why fluid inclusions with CO_2 are uncommon at typical porphyry Cu-Au-Mo deposits and occur only at some their representatives, for example, at those formed at deeper levels (e.g., Rusk et al., 2008). In contrast, both CO_2 and CH_4 are common in fluid inclusions at reduced intrusion-related Au deposits that are typically associated with plutons crystallized at greater depths (Baker, 2002).

These veins formed from a low-salinity (< 10 wt% NaCl-eq.), high-carbonic, methane-rich fluid, under its boiling and phase separation into essentially gaseous and liquid aqueous fluids. The respective subtype 4A and 4B fluid inclusions homogenize at 340–390 °C, and the younger type 5 fluid inclusions – at 295–250 °C, thus indicating a long-lasting fluid cooling during the vein formation. Gonevchuk et al. (2009) reported intermediate temperatures, thus supporting a continuity of these fluid inclusions types. The pressure of ~550 ± 50 bars at the temperature of 340–380 °C estimated for the type 4 fluid inclusions corresponds to a depth of ~2.2 km assuming lithostatic conditions (cf. Fournier, 1999), thus indicating a significant pressure drop as compared to that during the “porphyry cycle” at Lazurnoe, in turn suggesting a trend toward hydrostatic conditions, likely due to intense faulting and fracturing. However, despite of possibly shallower depths of formation of the late auriferous quartz-sulfide veins, their causative intrusions could have been emplaced and degassed at a greater depth (Fig. 13).

As a result, by structural setting, mineral composition and fluid inclusion characteristics, the late auriferous quartz-sulfide veins at Lazurnoe resemble those found in reduced intrusion-related Au deposits (Baker, 2002; Lang and Baker, 2001; Hart, 2007; Nevolko et al., 2019). Nearly-contemporaneous (to the porphyry Cu-Au-Mo mineralization at Lazurnoe) Early to early Late Cretaceous reduced intrusion-related Au and W deposits are present in the Central Sikhote-Alin (Sakhno et al., 2013; Gvozdev et al., 2016; Soloviev et al., 2017a,b; Ivin et al., 2017). This supports the possibility of a reduced ilmenite-series (or transitional ilmenite-magnetite series) plutonic suite, which would be parental for this type of mineralization at Lazurnoe. The orogenic gold model can be considered if the relationships of the late auriferous quartz-sulfide veins at Lazurnoe to any plutonic suite remain indistinct (Goldfarb et al., 2001), although Cretaceous and younger orogenic Au mineralization is not known in the region. Fluid boiling favored metal deposition (Drummond and Ohmoto, 1985). The reduced (pyrrhotite-stable) environment combined with an elevated fS_2 (indicated by arsenopyrite + pyrite association) also favored Au deposition at lower temperatures, as partitioning of Au in this process is essentially influenced by the behavior of sulfur, with lower redox conditions facilitating sulfide (bearing Au) precipitation from mineralized fluids (e.g., Lang and Baker, 2001; Yang, 2012).

10.6. Sulfur isotope data interpretation

The sulfur isotope data indicate relatively homogenous sulfur isotope values of sulfides from potassic, propylitic and phyllic alteration assemblages, with overall variations of $\delta^{34}S$ values from −1.9 to 3.4‰ (Table 4). The proximity to the meteorite standard supports a magmatic source of sulfur (Ohmoto and Goldhaber, 1997; Seal, 2006), whereas the homogeneity indicates sulfur isotope homogenization in a

magmatic chamber. On the other hand, there are distinct variations of $\delta^{34}S$ values that occur at the potassic, propylitic and phyllic alteration stages, with $\delta^{34}S$ values varying from slightly enriched in light sulfur isotope to those slightly enriched in heavy sulfur isotope at every hydrothermal stage. This can correspond to a systematic isotopic zonation around the mineralized core of porphyry Cu-Au-Mo deposits, with $\delta^{34}S$ values increasing from the internal toward external zones due to isotopic exchange between sulfate and sulfide sulfur and decreasing fO_2 (Ohmoto and Rye, 1979; Deyell, 2005; Deyell and Tosdal, 2005; Wilson et al., 2007). Consistently positive $\delta^{34}S$ values in minerals from the late auriferous quartz-sulfide veins indicate a distinct enrichment in heavy sulfur isotope that could be caused by sulfur sourcing from a more reduced source (e.g., ilmenite-series magmatic reservoir).

11. Conclusions

The Lazurnoe deposit is a significant emerging porphyry Cu-Au-Mo deposit in the Sikhote-Alin orogenic belt. It is located in a turbidite terrane, and was formed under the transform continental margin regime occurring in a regional zone of strike-slip fault. The deposit is related to a magnetite-series, high-K calc-alkaline to shoshonitic igneous suite occurring in a continental transform margin setting. The fertile magma was sourced from a subduction-modified mantle, under a low degree of partial melting, and was subjected to intense amphibole fractionation during its crystallization, the latter facilitating water and metal saturation in the evolving magma. The causative igneous suite dated at ~110–100 Ma was coeval to ilmenite-series calc-alkaline igneous suites that are accompanied by reduced intrusion-related Au (± W) to W-Au deposits as well as by Sn-W deposits. The deposit may represent part of a new large (region-scale) province of porphyry Cu-Au-Mo deposits related to the Early-early Late Cretaceous shoshonitic to calc-alkaline magmatism.

Magmatic crystallization was accompanied by the exsolution of metalliferous magmatic-hydrothermal fluids. Potassic alteration assemblages formed from a homogenous, high-salinity (45–48 wt% NaCl and 9–10 wt% $CaCl_2$), sodic-calcic aqueous-chloride fluid. Propylitic alteration assemblages formed from a homogenous sodic-calcic aqueous-chloride fluid that was characterized by a decreasing salinity (from 29 to 31 wt% NaCl and 18–19 wt% $CaCl_2$ through 24–25 wt% NaCl and 16–17 wt% $CaCl_2$ to 12 ± 0.5 wt% NaCl and 12 ± 0.5 wt% $CaCl_2$). Finally, phyllic alteration assemblages formed from a homogenous high-salinity (30–37 wt% NaCl and 5 ± 0.5 wt% $CaCl_2$) aqueous-chloride fluid thus suggesting another cycle of fluid exsolution from crystallizing magma. The porphyry-style assemblages are overprinted by the late auriferous quartz-sulfide veins containing arsenopyrite, pyrrhotite and other sulfide minerals, together with native gold and telluride mineralization. These veins were formed from boiling aqueous-carbonic fluid that was characterized by elevated CO_2 and CH_4 contents, with subsequent separation of high-carbonic and aqueous-chloride phases, and the fluid cooling from ~390 to 250 °C. These veins can be related to another, more reduced, plutonic suite.

The sulfur isotope data indicate relatively homogenous sulfur isotope values of sulfides from potassic, propylitic and phyllic alteration assemblages, with overall variations of $\delta^{34}S$ values close to meteoritic standard (from −1.9 to 3.4‰). This supports a magmatic source of sulfur, whereas the homogeneity indicates sulfur isotope homogenization in a magmatic chamber. Consistently positive $\delta^{34}S$ values in minerals from the late auriferous quartz-sulfide veins indicate a distinct enrichment in heavy sulfur isotope that could be caused by sulfur sourcing from a more reduced source (e.g., ilmenite-series magmatic reservoir).

Acknowledgments

This paper represents part of the authors' work on research and assessment of porphyry Cu-Au deposits in the Russian Far East. The authors are grateful to Alexander Efimov and Vasily Shapovalenko for fruitful discussions. The work was financially supported by the Program no. 72-4 of the Russian Academy of Sciences and the Scientific Program of IGEM RAS, and by the Contract no. 05-12/1 for the Project no. 1-33/12 of TsNIGRI. Special thanks are to the PrimorGeologiya State Enterprise for supporting fieldwork and providing access to the drill core and other data. Editorial reviews by Franco Pirajno, Hervé Rezeau, Alexander Yakubchuk and Ilya Prokopyev significantly improved the paper.

Appendix A. Supplementary data

Supplementary data to this article can be found online at https://doi.org/10.1016/j.oregeorev.2019.103063.

References

Atkinson, A.B., 2002. A model for the PTX properties of H_2O-NaCl. M.Sc.Thesis. Virginia Tech. Institute and State University, pp. 126.
Avilova, O.V., Andreev, A.V., Girfanov, M.M., Kryazhev, S.G., Starostin, I.A., 2016. Geological prospecting models for copper-porphyry and gold-polysulfide ore mineralization of the Sobolinoe perspective area, Sikhote-Alin Region. Ores Metals 2, 51–72 (in Russian).
Audetat, A., Pettke, T., Heinrich, C.A., Bodnar, R.J., 2008. The composition of magmatic-hydrothermal fluids in barren and mineralized intrusions. Econ. Geol. 103, 877–908.
Baker, T., 2002. Emplacement depth and carbon dioxide-rich fluid inclusions in intrusion-related gold deposits. Econ. Geol. 97, 1111–1117.
Bakker, R.J., 2003. Package FLUIDS 1. Computer programs for analysis of fluid inclusions data and for modeling bulk fluid properties. Chem. Geol. 194, 3–23.
Becker, S.P., Fall, A., Bodnar, R.J., 2008. Synthetic fluid inclusions. XVII. PVTX properties of high-salinity H_2O-NaCl solutions (> 30 wt.% NaCl): applications to fluid inclusions that homogenize by halite disappearance from porphyry copper and other hydrothermal ore deposits. Econ. Geol. 103, 539–544.
Belyansky, G.S., Rybalko, V.I., Syasko, A.A., Bazhanov, V.A., Uglova, N.I., Abramova, V.A., Oleinikov, A.B., Kovalenko, S.V., Kashtaev, B.I., Alenicheva, A.A., Gonokhova, N.G., 2011. Explanatory notes to the geological map of Russia, L-52/53, and K-52/53 map sheets, 1: 1,000,000 scale, 3rd generation. VSEGEI, St-Petersburg pp. 699(in Russian).
Bissig, T., Cooke, D.R., 2014. Introduction to the special issue devoted to alkalic porphyry Cu-Au and epithermal Au deposits. Econ. Geol. 109, 819–825.
Bodnar R.J., 1995. Fluid inclusion evidence for a magmatic source for metals in porphyry copper deposits. In: J.F.H. Thompson, J.F.H., Magmas, fluids, and ore deposits. Min. Assoc. Canada Short Course Series, v. 23, pp. 139–152.
Bodnar, R.J., Vityk, M.O., 1994. Interpretation of microthermometric data for H_2O-NaCl fluid inclusions. In: De Vivo, B., Frezzotti, M.L. (Eds.), Fluid inclusions in minerals, methods and applications. Blacksburg, Virginia Tech, pp. 117–130.
Bodnar, R.J., Burnham, C.W., Sterner, S.M., 1985. Synthetic fluid inclusions in natural quartz. III. Determination of phase equilibrium properties in the system H_2O-NaCl to 1000°C and 1500 bars. Geochim. Cosmochim. Acta 49, 1861–1873.
Borisenko, A.S., 1977. Study of the salt composition of solutions of gas-liquid inclusions in minerals by the cryometric method. Russ. Geol. Geophys. 8, 16–27.
Bukhanova, D.S., 2018. First data on the age of the Malmyzh copper-gold porphyry deposit, Khabarovsk Region. In: Petrov, V.A., Amplieva, E.E., Ustinov, S.A., Kovalchuk, E.V. (Eds.), New Data in the Understanding of the Mineral Formation Processes, 8th Youth Scientific-Practical School, 26-30 Nov. 2018. IGEM RAS, Moscow, pp. 81–82 in Russian.
Chappell, B.W., White, A.J.R., 1992. I- and S-type granites in the Lachlan Fold Belt. Trans. R. Soc. Edinburgh, Earth Sci. 83, 1–26.
Cline, J.S., Bodnar, R.J., 1994. Direct evolution of brine from a crystallizing silicic melt at the Questa, New Mexico, molybdenum deposit. Econ. Geol. 89, 1780–1802.
Cooke, D.R., Hollings, P., Walshe, J.L., 2005. Giant porphyry copper deposits: characteristics, distribution, and tectonic controls. Econ. Geol. 100, 801–818.
Cooke, D.R., Wilson, A.J., House, M.J., Wolfe, R.C., Walshe, J.L., Lickfold, V., Crawford, A.J., 2007. Alkalic porphyry Au-Cu and associated mineral deposits of the Ordovician to Early Silurian Macquarie Arc, New South Wales. Austr. J. Earth Sci. 54, 445–463.
Corbett. G.J., 2017. Epithermal Au-Ag and porphyry Cu-Au exploration. Short Course Manual, Sept. 2017 edition. http://www.corbettgeology.com.
M.L. Crawford, 1981. Phase equilibria in aqueous fluid inclusions. L.S. Hollister, M.L. Crawford (Eds.). Fluid inclusions: application to Petrology. Min Assoc Canada Short Course Handbook, Calgary 6, pp.75–100.
Darling, R.S., 1991. An extended equation to calculate NaCl contents from final clathrate melting temperatures in H_2O-CO_2-NaCl fluid inclusions: implications for PT-isochors location. Geochim. Cosmochim. Acta 55, 3869–3871.
Davidson, J., Turner, S., Handley, H., Macpherson, C., Dosseto, A., 2007. Amphibole "sponge" in arc crust? Geology 35, 787–790.
Davis, D.W., Lowenstein, T.K., Spencer, R.J., 1990. Melting behavior of fluid inclusions in laboratory-grown halite crystals in the systems NaCl–H_2O, NaCl–KCl–H_2O, NaCl–$MgCl_2$–H_2O, NaCl–$CaCl_2$–H_2O. Geochem. Cosmochim. Acta 54, 591–601.
Defant, M.J., Drummond, M.S., 1990. Derivation of some modern arc magmas by melting of young subducted lithosphere. Nature 347, 662–665.

Deyell, C.L., 2005. Sulfur isotope zonation at the Mt Polley alkalic porphyry Cu-Au deposit, British Columbia, Canada. In: Mao, J., Bierlein, F.P. (Eds.), Mineral Deposit Research: Meeting the Global Challenge. Springer, Berlin-Heidelberg, pp. 373–376.
Deyell C.L.R. Tosdal R., 2005. Sulfur isotopic zonation in alkalic porphyry Cu-Au systems: Applications to mineral exploration in British Columbia. B.C. Ministry of Energy and Mines, Geological Fieldwork Vol. 2004, pp. 191–208.
Drummond, S.E., Ohmoto, H., 1985. Chemical evolution and mineral deposition in boiling hydrothermal systems. Econ. Geol. 80, 126–147.
Efimov A.A., 2008. Report on the results of prospecting and assessment completed during 2005–2007 on the Lazurnoe copper-porphyry deposit and its flanks (Chuguev and Kavalerovo districts of the Primorie Region). Vladivostok, Shilka Minerals. pp. 135 (in Russian).
Fournier, R.O., 1999. Hydrothermal process related to movement of fluid from plastic into brittle rock in the magmatic-epithermal environment. Econ. Geol. 94, 1193–1212.
Garwin S., Hall R., Watanabe Y., 2005. Tectonic setting, geology, and gold and copper mineralization in Cenozoic magmatic arcs of southeast Asia and the west Pacific. Econ. Geology, 100th Anniv. Vol., pp.891–930.
Guo, Z., Wilson, M., Liu, J., Mao, Q., 2006. Post-collisional potassic and ultrapotassic magmatism of the northern Tibetan Plateau – Constraints on characteristics of the mantle source, geodynamic setting and uplift mechanisms. J. Petrol. 47, 1177–1220.
Goldfarb, R.J., Anderson, E.D., Hart, C.J.R., 2013. Tectonic setting of the Pebble and other copper-gold molybdenum porphyry deposits within the evolving middle Cretaceous continental margin of northwestern North America. Econ. Geol. 108, 405–419.
Goldfarb, R.J., Groves, D.I., Gardoll, S., 2001. Orogenic gold and geologic time: a global synthesis. Ore Geol. Rev. 18, 1–75.
Goldstein, R.H., Reynolds, T.J., 1994. Systematics of fluid inclusions in diagenetic minerals. Soc. Sediment Geol. Short Cour. 31 pp. 199.
Gonevchuk, V.G., Gonevchuk, G.A., Kokorin, A.M., Lebedev, V.A., Orekhov, A.A., 2005. New isotopic-geochronology data and some questions of the genesis of tin mineralization in the Kavalerovo district (Promorie Region, Russia). Pacific Geol. 24 (6), 77–87.
Gonevchuk, V.G., Gonevchuk, G.A., Korostelev, P.G., Semenyak, B.I., Seltmann, R., 2010. Tin deposits of the Sikhote-Alin and adjacent areas (Russian Far East) and their magmatic association. Aust. J. Earth Sci. 57 (6), 777–802.
Gonevchuk, V.G., Gonevchuk, G.A., Lebedev, V.A., Orekhov, A.A., 2011. Association of monzonitic rocks of the Kavalerovo ore district (Primorie): geochronology and some issues of genesis. Pacific Geol. 30 (3), 3–19 (in Russian).
Gonevchuk, V.G., Krylova, T.L., Orekhov, A.A., Gonevchuk, G.A., Kokorina, D.K., 2009. Peculiarities of fluid regime during formation of the systems with copper-molybdenum-gold and copper-tin mineralization (Iskra-Sobolinoe ore cluster of the Kavalerovo mineralized district, Primorie Region). Pacific Geol. 28 (1), 5–20 (in Russian).
Grebennikov, A.V., Khanchuk, A.I., Gonevchuk, V.G., Kovalenko, S.V., 2016. Cretaceous and Paleogene granitoid suites of the Sikhote-Alin area (Far East Russia): Geochemistry and tectonic implications. Lithos 261, 250–261.
Gregory, M.J., 2017. A fluid inclusion and stable isotope study of the Pebble porphyry copper-gold-molybdenum deposit. Alaska. Ore Geol. Rev. 80, 1279–1303.
Gustafson, L.B., Hunt, J.P., 1975. The porphyry copper deposit at El Salvador. Chile. Econ. Geol. 70, 857–912.
Gvozdev, V.I., Dobroshevskii, K.N., Vakh, A.S., Goryachev, N.A., Stepanov, V.A., Fedoseev, D.G., 2016. The Malinovskoe deposit as a new type of gold mineralization in the Primorie region, Russia (geology, mineralization, and genesis). Pacific Geol. 35 (1), 37–53 (in Russian).
Harris, A.C., Golding, S.D., 2002. New evidence of magmatic-fluid-related phyllic alteration: implications for the genesis of porphyry Cu deposits. Geology 30, 335–338.
Harris, A.C., Kamenetsky, V.S., White, N.C., Steele, D.A., 2004. Volatile phase separation in silicic magmas at Bajo de la Alumbrera porphyry Cu-Au deposit, NW Argentina. Resour. Geol. 54, 341–356.
Hart C.J.R., 2007. Reduced intrusion-related gold systems. In: Goodfellow W.D. (ed.), Mineral Deposits of Canada: A Synthesis of Major Deposit Types, District Metallogeny, the Evolution of Geological Provinces, and Exploration Methods. Geological Association of Canada, Mineral Deposits Division, Special Publication no. 5, pp. 95–112.
Hedenquist, J.W., Arribas, A., Reynolds, T.J., 1998. Evolution of an intrusion-centered hydrothermal system: Far Southeast-Lepanto porphyry and epithermal Cu-Au deposits. Philippines. Econ. Geol. 93, 373–404.
Hibbard, M.J., 1995. Petrography to Petrogenesis. Prentice Hall, New Jersey, pp. 587.
Holliday J.R., Cooke D.R., 2007. Advances in geological models and exploration methods for copper ± gold porphyry deposits. In: D. Milkereit (ed.), Proceedings of Exploration 2007: Fifth Internat.Conf. Min. Exploration, pp. 791–809.
Holtz, F., Becker, A., Freise, M., Johannes, W., 2001. The water-undersaturated and dry Qz-Ab-Or system revisited. Experimental results at very low water activities and geological implications. Contrib. Mineral. Petrol. 141, 347–357.
Hou, Z., Cook, N.J., 2009. Metallogenesis of the Tibetan collisional orogen: a review and introduction to the special issue. Ore Geol. Rev. 36, 2–24.
Hou, Z., Yang, Z., Qu, X., Meng, X., Li, Z., Beaudoin, G., Rui, Z., Gao, Y., Zaw, K., 2009. The Miocene Gangdese porphyry copper belt generated during post-collisional extension in the Tibetan Orogen. Ore Geol. Rev. 36, 25–51.
Hou, Z., Zhang, H., Pan, X., Yang, Z., 2011. Porphyry (Cu-Mo-Au) deposits related to melting of thickened mafic lower crust – examples from the eastern Tethyan metallogenic domain. Ore Geol. Rev. 39, 21–45.
Hou, Z., Ma, H., Zaw, K., Zhang, Y., Wang, M., Wang, Z., Pan, G., Tang, R., 2003. Himalayan Yulong porphyry copper belt - product of large-scale strike-slip faulting in eastern Tibet. Econ. Geol. 98, 125–145.
Ishihara, S., 1981. The granitoid series and mineralization. Econ. Geol. 75, 458–484.
Ivin, V.V., Rodionov, A.N., Medvedev, E.I., Fatyanov, I.I., 2017. Peculiarities of location of various precious mineralization in the Primorie region and its resource potential. Adv. Curr. Nat. Sci. Earth Sci. 8, 80–89 (in Russian).
Jahn, B.M., Valui, G., Kruk, N., Gonevchuk, V., Masako, U., Wu, J.T.J., 2015. Emplacement ages, geochemical, and Sr-Nd-Hf isotopic characterization of Mesozoic to Early Cenozoic granitoids of the Sikhote-Alin orogenic belt, Russian Far East: crustal growth and regional tectonic evolution. J. Asian Earth Sci. 111, 872–918.
Jenner, F.E., O'Neil, H.S.C., Arculus, R.J., Mavrogenes, J.A., 2010. The magnetite crisis in the evolution of arc-related magmas and the initial concentration of Au, Ag and Cu. J. Petrol. 51, 2245–2264.
Jensen, E.P., Barton, M.D., 2000. Gold deposits related to alkaline magmatism. Rev. Econ. Geol. 13, 279–314.
Jung, C., Jung, S., Hoffer, E., Berndt, J., 2006. Petrogenesis of Tertiary mafic alkaline magmas in the Hocheifel, Germany. J. Petrol. 47, 1637–1671.
Khanchuk, A.I., Kemkin, I.V., Kruk, N.N., 2016. The Sikhote-Alin orogenic belt, Russian South East: terranes and the formation of continental lithosphere based on geological and isotopic data. J. Asian Earth Sci. 120, 117–138.
Klemm, L.M., Pettke, T., Heinrich, C.A., Campos, E., 2007. Hydrothermal evolution of the El Teniente deposit, Chile: Porphyry Cu-Mo ore deposition from low-salinity magmatic fluids. Econ. Geol. 102, 1021–1045.
Kovalenko, V.I., Rub, M.G., Osipov, M.A., Gladkov, N.G., Efremova, S.V., Koval, P.V., Rub, A.K., Ryazantseva, M.D., Sherkhan, O., Yakimov, V.M., Yarmolyuk, V.V., 1988. The Ore Potential of Igneous Associations. Nauka Publishing, Moscow pp. 231 (in Russian).
Kouzmanov, K., Pokrovski, G.S., 2012. Hydrothermal controls on metal distribution in porphyry Cu (-Mo-Au) systems. In: Hedenquist, J.W., Harris, M., Camus, F. (Eds.), Geology and Genesis of Major Copper Deposits and Districts of the World: A Tribute to Richard H. Sillitoe. SEG Spec. Publ., pp. 573–618.
Kruk, N.N., Simanenko, V.P., Gvozdev, V.I., Golozubov, V.V., Kovach, V.P., Serov, P.A., Moskalenko, E.Yu., Kuibida, M.L., 2014. Geochemical characteristics and sources of the melts of the Early Cretaceous granitoids in the Samarga terrain (Sikhote-Alin). Russ. Geol.Geophys. 55, 276–302.
Le Maitre, R.W., Bateman, P., Dudek, A., Keller, J., Lameyre, J., Le Bas, M.J., Sabine, P.A., Schmid, R., Sorensen, H., Streckeisen, A., Wooley, A.R., Zanettin, B., 1989. A classification of igneous rocks and glossary of terms. Blackwell, Oxford, pp. 193.
Lang, J.R., Baker, T., 2001. Intrusion-related gold systems: the present level of understanding. Miner. Depos. 36, 477–489.
Lang, J.R., Gregory, M.J., Rebagliati, C.M., Payne, J.G., Oliver, J.L., Roberts, K., 2013. Geology and magmatic-hydrothermal evolution of the giant Pebble porphyry copper-gold-molybdenum deposit, southwest Alaska. Econ. Geol. 108, 437–462.
Lang J.R., Stanley C.R., Thompson H.F.H., 1993. A subdivision of alkalic porphyry Cu-Au deposits into silica-saturated and silica-undersaturated subtypes. In: Porphyry Copper-Gold Systems of British Columbia, MDRU, University of British Columbia, Annual Technical Report – Year 2, pp. 3.2–3.14.
Li, Y., Selby, D., Condon, D., Tapster, S., 2017a. Cyclic magmatic-hydrothermal evolution in porphyry systems: High-precision U-Pb and Re-Os geochronology constraints from the Tibetan Qulong porphyry Cu-Mo deposit. Econ. Geol. 112, 1419–1440.
Li, Y., Li, X.-H., Selby, D., Li, J.-W., 2017b. Pulsed magmatic fluid release for the formation of porphyry deposits: Tracing fluid evolution in absolute time from the Tibetan Qulong Cu-Mo deposit. Geol. Soc. America Bull. https://doi.org/10.1130/G39504.1.
Lowell, J.D., Guilbert, J.M., 1970. Lateral and vertical alteration-mineralization zoning in porphyry ore deposits. Econ. Geol. 65, 373–408.
Ludington S., Hammarstrom J.M., Robinson G.R. Jr., Mars J.C., Miller R.J., 2012. Porphyry copper assessment of the Tibetan Plateau, China. U.S. Geological Survey Scientific Investigations Report 2010-5090-F. pp. 63.
MacLean, W.H., Barrett, T.J., 1993. Lithogeochemical techniques using immobile elements. J. Geochem. Explor. 48, 109–133.
Malinovsky, A.I., 2011. Lithochemical composition of terrigenous rocks of the Zhuravlevka terrane (Sikhote-Alin) and its geodynamic interpretation. Proc. KRASRC 18 (2), 14–30 (in Russian).
Malinovsky, A.I., Golozubov, V.V., 2012. Structure, composition and formation environments of Lower Cretaceous sediments of the Zhuravlevka terrane (Central Sikhote-Alin). Lithol. Mineral Depos. 4, 399–424 (in Russian).
Maniar, P.D., Piccoli, P.M., 1989. Tectonic discrimination of granitoids. Geol. Soc. Am. Bull. 101, 635–643.
Martin, H., Smithies, R.H., Rapp, R., Moyend, J.F., Champion, D., 2005. An overview of adakite, tonalite–trondhjemite–granodiorite (TTG), and sanukitoid: relationships and some implications for crustal evolution. Lithos 79, 1–24.
Masterman, G.J., Cooke, D.R., Berry, R.F., Walshe, J.L., Lee, A.W., Clark, A.H., 2005. Fluid chemistry, structural setting, and emplacement history of the Rosario Cu-Mo porphyry and Cu-Ag-Au epithermal veins, Collahuasi District, Northern Chile. Econ. Geol. 100, 835–862.
McDonough, W.F., Sun, S.-S., 1995. The composition of the Earth. Chem. Geol. 120, 223–253.
Middlemost, E.A.K., 1997. Magmas. Rocks and Planetary Development, Longman, Harlow, pp. 299.
Mihalasky M.J., Ludington S., Alexeiev D.V., Frost T.P., Light T.D., Briggs D.A., Hammarstrom J.M., Wallis, J.C., with contributions from Bookstrom A.A. and Panteleyev A., 2015. Porphyry copper assessment of northeast Asia-Far East Russia and Northeasternmost China. U.S. Geological Survey Scientific Investigations Report 2010–5090–W, pp. 104.
Moritz, R., Rezeau, H., Ovtcharova, M., Tayan, R., Melkonyan, R., Hovamkimyan, S., Ramazanov, V., Selby, D., Ulianov, A., Chiaradia, M., Putlitz, B., 2016. Long-lived, stationary magmatism and pulsed porphyry systems during Tethyan subduction to

postcollision evolution in the southernmost Lesser Caucasus, Armenia and Nakhitchevan. Gondwana Res. 37, 465–503.
Muller D., Groves D.I., 2019. Potassic igneous rocks and associated gold-copper mineralization. Springer International Publishing AG, part of Springer Nature, Berlin-Heidelberg-New York, 5th ed. pp. 398.
Mutschler F.E., Mooney T.C., 1993. Precious-metal deposits related to alkalic igneous rocks: Provisional classification, grade-tonnage data and exploration frontiers. In: R. V. Kirkham, W.D. Sinclair, R.I. Thorpe, J.M. Duke, (eds.), Mineral Deposit Modeling: Geological Association of Canada, Special Paper 40, pp. 479–520.
Naidenko A.N., 2013. Information Geological Report on the 2013 Work Completed on Cu-Au-Mo Porphyry Mineralization in the Sobolinoe Perspective Area (Primorie Region). Unpubl. Prof. Report, OSV PrimorGeologiya. pp. 15 (in Russian).
Nevolko, P.A., Dung, P.T., Fominykh, P.A., Hoa, T.T., Anh, T.T., Phuong, N.G., 2019. Origin of the intrusion-related Lang Vai gold-antimony district (Northeastern Vietnam): Constraints from fluid inclusions study and C-O-S-Pb isotope systematics. Ore Geol. Rev. 104, 114–131.
Oakes, C.S., Bodnar, R.J., Simonson, J.M., 1990. The system NaCl-$CaCl_2$-H_2O: 1. The ice liquidus at 1 atm total pressure. Geochem. Cosmochim. Acta 54, 603–610.
Ohmoto, H., Goldhaber, M.B., 1997. Sulfur and carbon isotopes. In: Barnes, H.L. (Ed.), Geochemistry of Hydrothermal Ore Deposits, 3rd edn. John Wiley and Sons, New York, pp. 517–611.
Ohmoto, H., Rye, R.O., 1979. Isotopes of sulfur and carbon. In: Barnes, H.L. (Ed.), Geochemistry of Hydrothermal Ore Deposits, 2nd edn. Wiley, New York, pp. 509–567.
Pearce, J., 1996. Sources and settings of granitic rocks. Episodes 19, 120–125.
Pearce, J.A., Harris, N.B.W., Tindle, A.G., 1984. Trace element discrimination diagrams for the tectonic interpretation of granitic rocks. J. Petrol. 25 (4), 956–983.
Pearce, J.A., Peate, D.W., 1995. Tectonic implications of the composition of volcanic arc magmas. Ann. Rev. Earth Planet. Sci. 23, 251–285.
Peccerillo, A., Taylor, S.R., 1976. Geochemistry of Eocene calc-alkaline volcanic rocks from the Kastamonu area, Northern Turkey. Contrib. Mineral. Petrol. 58, 63–81.
Petrov, O.V., Kiselev, E.A., Morozov, A.F., Shpikerman, V.I., Zubova, T.N., Shatov, V.V., Zmievsky, Y.P., 2015. State geological mapping, an effective way to the discovery of giant deposits. Reg. Geol. Metall. 64, 5–10 (in Russian).
Pirajno, F., 2009. Hydrothermal Processes and Mineral Systems. Springer, Berlin.
Pirajno, F., 2010. Intracontinental strike-slip faults, associated magmatism, mineral systems and mantle dynamics: examples from NW China and Altay-Sayan (Siberia). J. Geodynam. 50, 325–346.
Popov, M.A., Petukhov, V.I., Garbuzov, S.P., 2016. Mineral resource base of the Primorie region (an overview). Trans. Engineering School, Far East Federal Univ., Russian.
Rezeau, H., Moritz, R., Wotzlaw, J.-F., Tayan, R., Melkonyan, R., Ulianov, A., Selby, D., d'Abzac, F.-X., Stern, R.A., 2016. Temporal and genetic link between incremental pluton assembly and pulsed porphyry Cu-Mo formation in accretionary orogens. Geology 44, 627–630.
Rezeau, H., Leuthold, J., Tayan, R., Hovakimyan, S., Ulianov, A., Kouzmanov, K., Moritz, R., 2018. Incremental growth of mid- to upper-crustal magma bodies during Arabia-Eurasia convergence and collision: A petrological study of the calc-alkaline to shoshonitic Meghri-Ordubad pluton (Southern Armenia and Nakhitchevan, Lesser Caucasus). J. Petrol. 59, 931–966.
Richards J.P., 1995. Alkalic-type epithermal gold deposits – a review. Min. Assoc. Canada Short Course Series 23, pp. 367–400.
Richards, J.P., 2009. Postsubduction porphyry Cu-Au and epithermal Au deposits – products of remelting subduction-modified lithosphere. Geology 37 (3), 247–250.
Richards, J.P., 2011a. Magmatic to hydrothermal metal fluxes in convergent and collided margins. Ore Geol. Rev. 40, 1–26.
Richards, J.P., 2011b. High Sr/Y arc magmas and porphyry Cu ± Mo ± Au deposits: Just add water. Econ. Geol. 106, 1075–1081.
Robinson, B.W., Kusakabe, M., 1975. Quantitative preparation of sulfur dioxide, for $^{34}S/^{32}S$ analyses, from sulfides by combustion with cuprous oxide. Anal. Chem. 47, 1179–1181.
Roedder, E., 1984. Fluid inclusions in minerals. Rev. Mineral. 12, 644 p.
Rusk, B.G., Reed, M.H., Dilles, J.H., 2008. Fluid inclusion evidence for magmatic-hydrothermal fluid evolution in the porphyry copper-molybdenum deposit at Butte. Montana. Econ. Geol. 103, 307–334.
Sakhno, V.G., Kovalenko, S.V., Alenicheva, A.A., 2011. Monzonitoid magmatism of the Lazurnoe copper-porphyry deposit by the results of U-Pb and K-Ar dating, and peculiarities of the ore-bearing magma genesis by the isotope-geochemical studies. Doklady Earth Sci. 438 (1), 82–90.
Sakhno, V.G., Stepanov, V.A., Gvozdev, V.I., Dobroshevskii, K.N., 2013. The Malinovka gold-bearing ore-magmatic system of central Sikhote Alin (Primor'e Region, Russia): geochronology, petrogeochemistry, and isotopic signatures of igneous complexes. Doklady Earth Sci. 452 (1), 887–894.
Samson, I.M., Walker, R.T., 2000. Cryogenic Raman spectroscopic studies in the system NaCl–$CaCl_2$–H_2O and implications for low-temperature phase behavior in aqueous fluid inclusions. Can. Mineral. 38, 35–43.
Schmidt, C., Bodnar, R.J., 2000. Synthetic fluid inclusions: XVI. PVTX properties in the system H_2O-NaCl-CO_2 at elevated temperatures, pressures, and salinities. Geochim. Cosmochim. Acta 64, 3853–3869.
Seal, R.R., 2006. Sulfur isotope geochemistry of sulfide minerals. Rev. Mineral. Geochem. 61, 633–677.
Seedorff, E., Dilles, J., Proffett, J.J., Einaudi, M., Zurcher, L., Stavast, W., Johnson, D., Barton, M., 2005. Porphyry deposits: charateristics and origin of hypogene features. Econ. Geol. 100, 251–298.
Shinohara, H., Hedenquist, J.W., 1997. Constraints of magma degassing beneath the Far Southeast porphyry Cu-Au deposit, Philippines. J. Petrol. 38, 1741–1752.
Sillitoe, R.H., 2002. Some metallogenic features of gold and copper deposits related to alkaline rocks and consequences for exploration. Miner. Depos. 37, 4–13.
Sillitoe, R.H., 2010. Porphyry copper systems. Econ. Geol. 105, 3–41.
Soloviev, S.G., 2014. The Metallogeny of Shoshonitic Magmatism. Moscow, Scientific World Publishing. V. 528 p., V. 2. 472 p. (in Russian).
Soloviev, S.G., Krivoschekov, N.N., 2011. The Vostok-2 gold-base metal-tungsten skarn deposit, Central Sikhote-Alin, Russia. Geol. Ore Depos. 6, 543–568.
Soloviev, S.G., Kryazhev, S.G., 2017. Geology, mineralization, and fluid inclusion characteristics of the Skrytoe reduced-type W skarn and stockwork deposit, Sikhote-Alin. Russia. Miner. Depos. 52 (6), 903–928.
Soloviev, S.G., Kryazhev, S.G., Dvurechenskaya, S.S., 2017a. Geology, mineralization, stable isotope, and fluid inclusion characteristics of the Vostok-2 reduced W-Cu skarn and Au-W-Bi-As stockwork deposit, Sikhote-Alin, Russia. Ore Geol. Rev. 86, 338–365.
Soloviev, S.G., Kryazhev, S.G., Dvurechenskaya, S.S., 2017b. Geology, mineralization, and fluid inclusion characteristics of the Lermontovskoe reduced-type tungsten (± Cu, Au, Bi) skarn deposit, Sikhote-Alin, Russia. Ore Geol. Rev. 89, 15–39.
Soloviev, S.G., Kryazhev, S.G., Dvurechenskaya, S.S., 2018. Geology, mineralization, and fluid inclusion study of the Kuru-Tegerek Au-Cu-Mo skarn deposit in the Middle Tien Shan, Kyrgyzstan. Miner. Depos. 53 (2), 195–223.
Soloviev, S.G., Kryazhev, S.G., Dvurechenskaya, S.S., Vasyukov, V.E., Shumilin, D.A., 2019. The superlarge Malmyzh Cu-Au porphyry deposit, Sikhote-Alin, Eastern Russia: Igneous geochemistry, hydrothermal alteration, mineralization, and fluid inclusion characteristics. Ore Geol Reviews (submitted).
Sun, W.D., Huang, R.F., Li, H., Hu, Y.B., Zhang, C.C., Sun, S.J., Zhang, L.P., Ding, X., Li, C.Y., Zartman, R.E., Ling, M.X., 2015. Porphyry deposits and oxidized magmas. Ore Geol. Rev. 65, 97–131.
Sun, S.-S., McDonough, W.F., 1989. Chemical and isotopic systematics of oceanic basalts: Implications for mantle composition and processes. Geol. Soc. London, Specl. Publicat. 42, 313–345.
Thiéblemont, D., Tegyey, M., 1994. Une discrimination géochimique des roches différenciées témoin de la diversité d'origlisboaine et de situation tectonique des magmas calcoalcalins. Comptes Rendus de l'académie des Sciences Paris 319, 87–94.
Thiery, R., Kerkhof, A.M., Dubessy, J., 1994. νX properties of CH_4-CO_2 and CO_2-N_2 fluid inclusions: modeling for T < 31 °C and P < 400 bars. Europ. J. Mineral. 6, 753–771.
Tsuruoka, S., 2017. The Evolution of Hydrothermal Fluids from the Deep Porphyry Environment to the Shallow Epithermal Environment. Ph. D. Dissertation. Colorado School of Mines, pp. 196.
Vanko, D.A., Bodnar, R.J., Sterner, S.M., 1988. Synthetic fluid inclusion: VIII. Vapor-saturated halite solubility in part of the system NaCl-$CaCl_2$-H_2O, with application to fluid inclusions from oceanic hydrothermal systems. Geochim. Cosmochim. Acta 52, 2451–2456.
Vasilenko, G.P., 2004. The Dalnegorsk ore district. In: Khanchuk, A.I., Gonevchuk, G.A., Seltmann, R. (Eds.), Metallogeny of the Pacific Northwest (Russian Far East): tectonics, magmatism and metallogeny of active continental margins. Guidebook for the Field Excursions in the Far East of Russia: Sept. 1-20, 2004. Dalnauka, Vladivostok, pp. 98–124.
Wallace, P., Carmichael, I.S.E., 1992. Alkaline and calcalkaline lavas near Los Volcanes, Jalisco, Mexico – geochemical diversity and its significance in volcanic arcs. Contrib. Mineral. Petrol. 111, 423–439.
Williamson, B.J., Herrington, R.J., Morris, A., 2016. Porphyry copper enrichment linked to excess aluminum in plagioclase. Nat. Geosci. 9. https://doi.org/10.1038/ngeo2651.
Wilson, A.J., Cooke, D.R., Harper, B.L., 2003. The Ridgeway gold-copper deposit; a high-grade alkalic porphyry deposit in the Lachlan fold belt, New South Wales, Australia. Econ. Geol. 98, 1637–1666.
Wilson, A.J., Cooke, D.R., Harper, B.J., Deyell, C.L., 2007. Sulfur isotopic zonation in the Cadia district, southeastern Australia: exploration significance and implications for the genesis of alkalic porphyry gold-copper deposits. Miner. Depos. 42, 465–487.
Yang, X.-M., 2012. Sulfur solubility in felsic magmas: implications for genesis of intrusion-related gold mineralization. Geosci. Canada 39, 17–32.
Yang, Z., Hou, Z., Chang, Z., Li, Q., Liu, Y., Qu, H., Sun, M., Xu, B., 2016. Co-spatial Eocene and Miocene granitoids from the Jiru Cu deposit in Tibet: Petrogenesis and implications for the formation of collisional and post-collisional porphyry Cu systems in continental collision zones. Lithos 245, 243–257.
Yushmanov, Y.P., 2001. Structural control on gold mineralization of the Sobolinoe ore district in the Central Sikhote-Alin. Natl. Geol. 3, 15–17 (in Russian).
Yushmanov, Y.P., 2002. Structure and zonation of Cu-Au mineralization at the Lazurnoe deposit in the Central Sikhote-Alin. Pacific Geol. 21 (2), 85–90 (in Russian).
Yushmanov, Y.P., 2009. Geology, Structure and Metallogeny of the Sobolinoe Ore District (Primorie). DVGSGA Publishing, Birobidzhan, pp. 62 (in Russian).
Zhang, Z., Xiao, X., Wang, J., Wang, Y., Kusky, T.M., 2008. Postcollisional Plio-Pleistocene shoshonitic volcanism in the western Kunlun Mountains, NW China: geochemical constraints on mantle source characteristics and petrogenesis. J. Asian Earth Sci. 31, 379–403.
Zhao, J., Zhou, M., 2009. Secular evolution of the Neoproterozoic lithospheric mantle underneath the northern margin of the Yangtze block, South China. Lithos 107, 152–168.
Zhou, Y., Xu, B., Zeng-Qian Hou, Z.-Q., Wang, R., Zheng, Y.-C., He, W.-Y., 2019. Petrogenesis of Cenozoic high–Sr/Y shoshonites and associated mafic microgranular enclaves in an intracontinental setting: Implications for porphyry Cu-Au mineralization in western Yunnan, China. Lithos 324-325, 39-54.